Science of the Total Environment

A facile and sensitive hexahomotrioxacalix[3]arene-based fluorescent sensor for the detection of trace amounts of 2,4,6-trinitrophenol

--Manuscript Draft--

Manuscript Number:	STOTEN-D-23-29602R1
Article Type:	Research Paper
Keywords:	Fluorescent sensor, Hexahomotrioxacalix[3]arene, Click reaction, Trinitrophenol detection.
Corresponding Author:	Chong Wu Guizhou University of Traditional Chinese Medicine CHINA
First Author:	Yong-Lang Liu
Order of Authors:	Yong-Lang Liu
	Lu-Fang Wu
	Chong Wu
	Shofiur Rahman
	Abdullah Alodhayb
	Carl Redshaw
	Paris Georghiou
	Takehiko Yamato
Abstract:	Nitroaromatic compounds are common explosives and toxic pollutants, the selective and sensitive detection of which is of great importance. Herein, a facile and sensitive fluorescent sensor L was constructed for the sensing of TNP based on the hexahomotrioxacalix[3]arene skeleton. The fluorescence emission of L was drastically quenched in the presence of 2,4,6-trinitrophenol (TNP), while other tested NACs, metal ions, and anions induced negligible changes. Under the optimized conditions, the spectroscopic studies revealed that L exhibited extremely sensitive and selective TNP recognition, with a detection limit of 9.17 × 10-7 M and a quenching constant of 2.44 × 104 M-1. The sensitivity of sensor L for TNP was attributed to the formation of a ground-state charge-transfer complex and an inner filter effect, which also contributed to the special selectivity of the sensor among the various nitroaromatic analogues. Compared with previous reports, L can serve as a highly efficient sensor for the sensing of TNP and can be employed over a wide pH range of 2 to 12. Sensor L was effectively used to quantify TNP in real water and soil samples. Additionally, fluorescent test strips were also developed for visual and rapid detection of TNP in both the solution and vapour phases.
Response to Reviewers:	

Dear editor Prof. Barceló,

Thank you very much for your consideration of our manuscript entitled "*A facile and sensitive hexahomotrioxacalix[3]arene-based fluorescent sensor for the on-site monitoring trace 2,4,6-trinitrophenol*", (Manuscript ID: STOTEN-D-23-29602.) We appreciate the constructive comments and suggestions from you and the reviewers.

In Particular, according to the suggestions from the reviewer #3, the keywords "on-site monitoring" in the title of our manuscript was deleted, and the title is now revised as "*A facile and sensitive hexahomotrioxacalix[3]arene-based fluorescent sensor for the detection of trace amounts of 2,4,6-trinitrophenol*". We have revised our manuscript, addressed the reviewers' concerns and have formatted the manuscript as requested. We hope that this revised manuscript resolves all the issues the referees may have. At the end of this letter, please find our detailed response to all the questions point by point, which are highlighted in green in the manuscript. We hope the revised paper would now satisfy you and the reviewers.

Thank you very much for your time and consideration.

Yours faithfully,

Dr. Chong Wu

Guizhou University of Traditional Chinese Medicine

Tel: (0086) 18886092015

E-mail: wuchongchem@163.com

A facile and sensitive hexahomotrioxacalix[3]arene-based fluorescent sensor for the detection of trace amounts of 2,4,6-trinitrophenol

Yong-Lang Liu[a], Lu-Fang Wu[a], Chong Wu[a,b]*, Shofiur Rahman[c], Abdullah Alodhayb[c], Carl Redshaw[d], Paris E. Georghiou[e,]* and Takehiko Yamato[b,]*

[a]College of Pharmacy, Guizhou University of Traditional Chinese Medicine, Guiyang 550025, China

[b]Department of Applied Chemistry, Faculty of Science and Engineering, Saga University, Saga 840-8502, Japan

[c]Biological and Environmental Sensing Research Unit, King Abdullah Institute for Nanotechnology, King Saud University, Riyadh 11451, Saudi Arabia

[d]Chemistry, School of Natural Sciences, The University of Hull, Hull, HU6 7RX, UK

[e]Department of Chemistry, Memorial University of Newfoundland, St. John's, A1B3X7, Canada.

*Corresponding authors: wuchongchem@163.com (C. Wu), yamatot@cc.saga-u.ac.jp (T. Yamato), parisg@mun.ca (P.E. Georghiou).

Reviewer(s)' Comments to Author:

Reviewer #2:

Prof. Wu and coworkers have reported one novel fluorescent sensor for detecting and quantifying harmful 2,4,6-trinitrophenol pollutant using supramolecular hexahomotrioxacalix[3]arene. This manuscript has provided one convenient and efficient test strip which could be fabricated for on-site visual detection of TNP in both solution and vapor phase. Overall this article will be of great interest for many scientists; hence, this manuscript need a minor improvement before it can be published in Science of the Total Environment. The following specific comments should be taken into account:

(1) Although the sensor L has been fully characterized by 1H/13C NMR and HRMS, the cited reference (Ni et al., 2012) doesn't demonstrate the synthesis procedure for crucial intermediate compound 3. Thus, the author should cite a correct ref. or describe the synthesis procedure in detail.

Response: We thank the referee and have now added a detailed synthesis procedure for compound 3.

(2) In the synthesis and characterization part, the 1H NMR assignment should be given.

Response: We thank the referee and have now added the 1H NMR assignment for all the compounds synthesized in this work.

(3) 'Click' is not a proper noun, therefore it should not be capitalized unless at the beginning of a sentence.

Response: We have modified the manuscript accordingly.

(4) The TOC of this manuscript is strongly recommended for redrawing and redesigning.

Response: Thank the referee very much for the comment and have now improved the TOC.

Reviewer #3:

It is a very well written paper but there are some comments concerning on-site monitoring: The keyword On-site Monitoring should be withdrawn because the are no validation of data of real world samlples and no matrix effects are discussed. There are some spiked test samlples and recoveries given. But this should be investigated and validated with real water samples in the environmental matrix. May be the authors do have some valid field data concerning on-site monitoring - these data should be added if available.

Response: Sincerely thank the referee for positive comments on this work. The suggestions have been helpful in revising and improving our manuscript. We selected three real environment samples (including tap water, pond water, and soil) to verify the feasibility of present spectrofluorimetric method. Meanwhile, the conventional HPLC experiments were also conducted on the same samples to verify the reliability. Considering the fast response of sensor **L** to TNP, a convenient fluorescent test strips was also fabricated for visual rapid detection of TNP in real samples. Based on the above discussion, we have removed the keyword “on-site monitoring”.

A facile and sensitive hexahomotrioxacalix[3]arene-based fluorescent sensor for the detection of trace amounts of 2,4,6-trinitrophenol

Abstract:

Nitroaromatic compounds are common explosives and toxic pollutants, the selective and sensitive detection of which is of great importance. Herein, a facile and sensitive fluorescent sensor **L** was constructed for the sensing of TNP based on the hexahomotrioxacalix[3]arene skeleton. The fluorescence emission of **L** was drastically quenched in the presence of 2,4,6-trinitrophenol (TNP), while other tested NACs, metal ions, and anions induced negligible changes. Under the optimized conditions, the spectroscopic studies revealed that **L** exhibited extremely sensitive and selective TNP recognition, with a detection limit of 9.17×10^{-7} M and a quenching constant of 2.44×10^{4} M^{-1}. The sensitivity of sensor **L** for TNP was attributed to the formation of a ground-state charge-transfer complex and an inner filter effect, which also contributed to the special selectivity of the sensor among the various nitroaromatic analogues. Compared with previous reports, **L** can serve as a highly efficient sensor for the sensing of TNP and can be employed over a wide pH range of 2 to 12. Sensor **L** was effectively used to quantify TNP in real water and soil samples. Additionally, fluorescent test strips were also developed for visual and rapid detection of TNP in both the solution and vapour phases.

Keywords: Fluorescent sensor, Hexahomotrioxacalix[3]arene, Click reaction, Trinitrophenol detection.

1 Introduction

Nitroaromatic compounds (NACs) are the major components of explosives. NACs, including TNP, are also common chemical reagents that are extensively used in the wider chemical, pharmaceutical, leather and dye industries (Zan et al., 2022). However, as a result of its widespread use, as well as in explosives, once TNP in particular is released into the environment, due to its high solubility in water, it readily contaminates soil and aquatic systems (Liu et al., 2022a). Furthermore, due to its electron-deficient nature, TNP is difficult to be degraded in both biosystems and the environment, thus becoming one of the major environmental pollutants (Kumar et al., 2023). Significantly, TNP exhibits various toxic effects towards living organisms, such as carcinogenicity, mutagenicity, liver damage, skin irritation, etc (Goel and Malhotra, 2022). Consequently, the United States Environmental Protection Agency (EPA) included TNP in its list of priority pollutants (Ilyas et al., 2022). It is therefore of significant interest and relevance to develop accurate and sensitive analytical methods for the selective detection of TNP.

To date, many analytical techniques have been developed to detect NACs, such as HPLC (Gledhill et al., 2019), GC-MS (Weiss et al., 2004), ion mobility spectroscopy (Kostarev et al., 2022), surface-enhanced Raman spectroscopy (Wang et al., 2022), electrochemistry analysis (Zheng et al., 2023) and fluorescence spectroscopy (Liu et al., 2022b). Among these various methods, fluorescence based sensing methodologies have proven to be excellent candidates by virtue of their excellent selectivity and sensitivity, short response time, real-time monitoring, and operational simplicity (Harathi and Thenmozhi, 2022; Qu et al., 2020). In this regard, fluorescent materials including conjugated polymers (Nguyen et al., 2023), supramolecular ensembles (Hu et al., 2023), MOFs (Kaur et al., 2023), COFs (Zhu et al., 2022), AIEgens (Wang et al., 2020a), small organic molecules (Thippeswamy et al., 2022), nanoparticles (Kayhomayun et al., 2022), nanoclusters (Bener et al., 2022), carbon

dots (Wang et al., 2019), and quantum dots (Mukherjee et al., 2022) have been developed for the detection of NACs.

The click reaction has been extensively employed to synthesize a wide range of 1,2,3-triazole-based fluorescent sensors that have been developed for the sensing of ionic species (Lau et al., 2011; Bryant and Bunz, 2013; Ahmed and Xiong, 2021). Nevertheless, these fluorescence systems have scarcely been specifically designed for the detection of NACs. The 1,2,3-triazole ring possesses three nitrogen atoms and thus, their lone pair electrons can coordinate to metal ions, and can be hydrogen bond and/or proton acceptor(s). On the other hand, NACs commonly function as electron acceptors owing to the electron-withdrawing nature of the nitro group(s) (Gole et al., 2011). As a result, significant noncovalent interactions may be formed between 1,2,3-triazole and NACs. These factors inspired us to design an efficient fluorescent sensor for sensing NACs via the click reaction.

In connection with our ongoing research on sensors for environmentally and biologically important guest species (Wu et al., 2023; Xie et al., 2020; Wu et al., 2018), herein, we report a novel hexahomotrioxacalix[3]arene-based sensor **L** with preorganized triazoles as recognition sites and has pendant pyrenes as the fluorophores for the fluorometric and colorimetric sensing of TNP. The sensing mechanism was systematically investigated by UV-vis/fluorescence titrations, fluorescence lifetime measurements, ^{1}H NMR spectroscopic titration analysis, and DFT caculations. Sensor **L** was successfully employed to detect TNP in actual water and soil samples with satisfactory results. As well, fluorescent test strips were also fabricated for the convenient and cost-effective real-time monitoring of TNP. The findings of this work present an appropriate strategy for the design and fabrication of fluorescent sensors for the rapid identification and quantification of the potentially TNP pollutant.

2 Experimental

2.1 Materials

All reagents were obtained from commercial suppliers and utilised without additional purification. NMR spectra were measured on a Bruker 400 MHz instrument. HRMS spectra were recorded using a mass spectrometer (Agilent 6540 Q-TOF). Fluorescence spectra were performed on a Shimadzu RF-5301PC spectrometer. Quantum yields were measured using absolute method using a Hamamatsu C11347-11 Quantaurus-QY Analyzer. Fluorescence lifetimes were determined on the Edinburgh FLS1000 steady-state transient fluorescence spectrometer. UV-vis spectra were taken on a Shimadzu UV-2600 UV-vis spectrometer. HPLC analysis was carried out on Agilent 1290 II-6460.

2.2 Synthesis and Characterization

The 1-azidomethylpyrene (Park et al., 2008) and precursors **1**, **2** (Ni et al., 2012) were produced according to the reported procedures. A suspension of compound **2** (890 mg, 1.0 mmol) and K_2CO_3 (1.24 g, 9.0 mmol) was heated at reflux for 1 h in dry acetone (80 mL), then propargyl bromide (480 mg, 4.0 mmol) was added, and the reaction mixture was refluxed for 24 h. After that, the reaction was cooled to room temperature, and the filtrate was concentrated. The residue was purified by column chromatography (dichloromethane as eluent) to afford the desired compound **3** (750 mg, 75 %). ^{1}H NMR (400 MHz, $CDCl_3$): δ = 7.58 (s, 6H, ArH_{calix}), 4.87–4.91 (d, 6H, J = 13.2 Hz, Ar$CH_{2(eq)}$O), 4.86 (s, 6H, OCH_2-alkynyl), 4.66 (s, 6H, ArOCH_2), 4.49–4.52 (d, 6H, J = 13.2 Hz, Ar$CH_{2(ax)}$O), 3.28–3.41 (dq, 12H, N$CH_2$$CH_3$), 2.51 (s, 3H, C≡$CH$), 1.12–1.21 (dt, 18H, N$CH_2$$CH_3$). ^{13}C NMR (100 MHz, $CDCl_3$) δ = 166.84, 164.72, 159.90, 132.03, 131.86, 125.08, 78.13, 74.72, 72.26, 68.93, 52.19, 41.06, 40.11, 14.32, 12.98. HRMS (FAB$^+$): calcd. for $[C_{54}H_{64}N_3O_{15} + H]^+$ 994.4337; found 994.4335.

A well-stirred solution of Compound **3** (500 mg, 0.50 mmol), 1-azidomethylpyrene (425 mg, 1.65 mmol), and CuI (30 mg) in 50 mL of THF/H_2O (4:1) was refluxed for 24 h. The solvent was removed, and the resulting residue was subsequently purified via column

chromatography (ethyl acetate as eluent) to afford **L** as white solid (600 mg, 68 %). ^{1}H NMR (400 MHz, $CDCl_3$): δ = 8.03–8.05 (d, 3H, *J* = 8.0 Hz, Py-*H*), 7.93–7.95 (d, 3H, *J* = 8.0 Hz, Py-*H*), 7.87–7.89 (d, 3H, *J* = 8.0 Hz, Py-*H*), 7.68–7.81 (m, 21H, Py-*H* (18H) and triazole-*H* (3H); overlapped), 7.12 (s, 6H, ArH_{calix}), 5.96 (s, 6H, triazole-CH_2-Py), 5.18 (s, 6H, OCH_2-triazole), 4.58–4.60 (d, 6H, *J* = 12.8 Hz, Ar$CH_{2(eq)}$O), 4.45 (s, 6H, ArOCH_2), 3.93–3.95 (d, 6H, *J* = 12.8 Hz, Ar$CH_{2(ax)}$O), 3.18–3.34 (dq, 12H, N$CH_2$$CH_3$), 1.06–1.12 (q, 18H, NCH_2CH_3). ^{13}C NMR (100 MHz, $CDCl_3$) δ = 166.81, 165.21, 159.96, 143.54, 131.77, 131.70, 131.57, 130.72, 130.13, 128.51, 127.75, 127.40, 126.85, 126.79, 125.88, 125.42, 125.32, 124.71, 124.61, 124.48, 124.36, 123.99, 121.76, 71.96, 68.68, 57.97, 51.94, 40.89, 39.96, 14.21, 12.91. HRMS (FAB$^+$): calcd. for $[C_{105}H_{96}N_{12}O_{15} + H]^+$ 1766.7230; found 1766.7228.

2.3 UV-vis and fluorescence titrations

Both the sensor **L** and the analytes were prepared as 1 mM stock solutions by dissolving them in acetonitrile. The stock solutions were diluted to the appropriate concentration with acetonitrile and buffer solutions. In titration experiments, a 3 mL solution of **L** was typically added to a quartz cuvette, followed by the addition of various stock solutions of analytes using a micro-syringe. Each titration was replicated three times in order to obtain consistent results.

2.4 Fluorescence sensing of TNP in real samples

Prior to usage, the crude water samples were filtered via a 0.22 μm membrane filter. The pH of the water samples was adjusted to 7.4 with HEPES buffer, and then different amounts of TNP were added. The obtained samples underwent further treatment using **L** and CH_3CN, resulting in the formation of final mixtures containing 50% CH_3CN. Subsequently, the fluorescence spectra of the mixes comprising **L** (with a final concentration of 1.0 μM) and TNP were recorded within 30 seconds. For the soil sample analysis, 1 g of soil samples were mixed with 1.0 mg and 2.0 mg of TNP, respectively, and subsequently dissolved in 100 mL deionized water. The soil samples were then filtered through a 0.22 μm membrane filter after

being ultrasonically treated for 15 minutes. Then, the fluorescence was measured after the stock solution of **L** (with a final concentration of 1.0 μM) was introduced.

2.5 HPLC analysis

For HPLC analysis, the C18 column (250×4.6 mm^2 id, 5 μm) was used as a stationary phase and 357 nm was chosen as detection wavelength. The mobile phase consisted of a mixture of methanol and 0.2% acetic acid in a 50:50 ratio. The temperature of the column was kept at 40 °C.

2.6 Fluorescent Test Strips

Fluorescent test strips were fabricated through the immersion of filter paper into the dichloromethane solution of **L**, followed by subsequent air drying. The detection method involved immersing the test papers into an aqueous solution of TNP, followed by drying and then observation under a 365 nm UV light.

3 Results and discussion

3.1 Synthesis

The synthetic pathway of sensor **L** is outlined in Scheme 1. The calixarene skeleton was fixed in the *cone* conformation by first introducing N,N-diethylamide by O-alkylation of the hydroxyl groups located at the lower-rim of the hexahomotrioxacalix[3]arene **1**. Subsequent base hydrolysis of the upper-rim ester yielded the corresponding triacid derivative **2**, and the intermediate **3** was successfully synthesized by employing propargyl bromide in the presence of K_2CO_3 as base. Submitting 1-azidomethylpyrene to a Cu(I)-catalyzed 1,3-dipolar cycloaddition reaction with compound **3** at click conditions resulted in a 68% yield of the sensor **L**. All chemicals synthesised in this study were completely characterised by ^{1}H and ^{13}C NMR spectroscopy, and HRMS (Fig.S1–S3).

3.2 Luminescent properties and detection of TNP

In order to obtain the optimal conditions for analytical applications, the fluorescence characteristics of compound **L** were examined in various solvent mixtures. As shown in Fig.S4, **L** emitted much stronger fluorescence in the CH_3CN/H_2O mixed solvents. In addition, the emission spectra of **L** were recorded by introducing varying water fractions (f_w) into the CH_3CN solution. As can be seen from Fig.S5, the fluorescence intensity enhanced gradually when f_w increases from 0% to 60%. However, a significant fluorescence decrease can be observed when the water content exceeds 70%. Subsequently, an assessment was conducted to examine the impact of pH on the fluorescence signals of **L**. This was achieved by altering the pH values within the range of 2.0 to 12.0. Fluorescence signals exhibited little variation with alteration of pH throughout the range of 5.0 to 12.0 (Fig.S6). Based on the above experimental findings, the CH_3CN/HEPES (v/v, 1:1, pH=7.4) system was applied in the experiments that followed.

The photophysical properties of **L** were studied by the absorption and fluorescence spectra in a 1:1 CH_3CN/HEPES pH=7.4 mixed solvent system (Fig.S7). The UV-vis absorption spectrum of **L** shows two absorption peaks characteristic of pyrene at 328 nm and 343 nm. The most intense absorption maximum (λ_{abs}) was observed at 343 nm, and the molar absorption coefficient (ε) was 8.58×10^4 L mol^{-1} cm^{-1}. Upon excitation at 343 nm, the emission spectra of **L** exhibits a prominent excimer emission at 484 nm arising from the intramolecular π-stacked pyrene units, with a quantum yield (φ) of 0.22. To evaluate the sensing ability of the designed receptor **L** in detecting NACs, we conducted preliminary fluorescence titration studies against TNP. The excimer emissions were efficiently quenched upon the incremental addition of TNP, and the shapes of the emission spectra did not significantly change (Fig.1). Meanwhile, the quenching in the fluorescence emission could be readily observed when illuminated with a UV lamp at 365 nm. To compare the sensing

selectivity of **L** toward TNP, fluorescence titration experiments using **L** were also performed with other NACs and potential interferents, including metal ions and anions. The results presented in Fig.2 and Fig.S8 demonstrate that the relative quenching efficiencies of different analytes towards sensor **L** are barely affected, implying that **L** may be potentially usable for TNP detection in actual samples. Among the tested analytes, it is worth noting that only TNP demonstrated a significant quenching efficiency, and the initial fluorescence intensity of **L** decreased by 93.2% when only 200 μM TNP was added. The calibration curve obtained for TNP exhibits clear linearity within the concentration range of 0 to 50 μM. Thus, the given TNP determination method achieved a detection limit of 9.17×10^{-7} M and a quantitation limit of 3.06×10^{-6} M, especially the precision (RSD%) was found to be 0.33% (Fig.S9). Significantly, the degree of emission quenching observed at the 10-second interval was nearly identical to that observed after a 24-hour period (Fig.S10), confirming the fast response and the stability of present system. This system therefore represents a fluorescent sensor that can be used to determine the concentration of TNP quantitatively.

Subsequently, UV-vis absorption titration experiments were also investigated to assess whether **L** could serve as a colorimetric sensor for TNP. As depicted in Figure 3, a notable increase in the initial absorption intensity was observed when TNP was gradually introduced into the solution of **L**. In the meanwhile, it was observed that the solution underwent a distinct and readily observable alteration in hue, transitioning from a state of transparency to a reddish orange appearance (Fig.3, inset). A linear correlation was observed between the concentration of TNP and the absorption intensity over the range of 0 to 160 μM (Fig.S11). This means that in addition to its use as a fluorescence sensor, **L** can also be a reliable colorimetric sensor for the detection of TNP at low concentrations. Significantly, in terms of selectivity, sensitivity, and limit of detection, **L** acts as a more sensitive TNP sensor than many other sensors that have been described thus far (Table S1).

3.3 The mechanism for the sensing of TNP with L

To better understand the quenching behavior exhibited by sensor **L** when exposed to TNP, the quenching mechanism needs to be well corroborated. Quenching can manifest through multiple mechanisms, typically categorised as static quenching and dynamic quenching. By using the Stern-Volmer equation ($I_0/I = 1 + K_{SV}[Q]$) to fit the observed data, we were able to get insight into the specifics of the quenching process in **L**. As depicted in Fig.S12, the Stern-Volmer plot exhibits a linear trend at low concentrations (up to 50 μM) and a non-linear upward curving at higher quencher concentrations. The linear regression analysis of the plot obtained at lower concentrations yielded a quenching constant of 2.44×10^4 M^{-1} for TNP. This result suggests that sensor **L** has a considerable quenching effect on TNP. Generally, a linear Stern–Volmer plot represents a singular (static or dynamic) quenching mechanism, whereas a positive deviation from linearity suggests the existence of a combined quenching process involving both static and dynamic mechanisms (Sun et al., 2015). The nature of Stern–Volmer plot in the present system falls into the latter category, indicating that a combination of quenching processes contribute to the emission quenching. In order to clarify which factor is the dominant one, time-resolved fluorescence measurements were conducted in the absence and presence of TNP. The lifetime decay plot of **L**, as depicted in Fig.S13, demonstrated that the introduction of TNP in a sequential manner resulted in negligible changes to the fluorescence lifetime. The average lifetime value (τ) of **L** at 484 nm (λ_{ex} = 343 nm) was found to be 141.45 ± 0.22 ns, further addition of 25 and 50 equivalents of TNP into the solution of **L** gave lifetime values of 140.89 ± 0.14 and 140.54 ± 0.18 ns, respectively. In the static mechanism, it can be observed that the fluorescence lifetime remains unaffected. This is due to the binding of the quencher with the sensor in its ground state, resulting in the formation of a non-fluorescent complex or "dark state" with the quencher. Consequently, the molecules that are not bound exhibit their inherent lifetimes. In contrast, the fluorescence lifespan of the dynamic mechanism is expected to decrease as a result of diffusive collisions occurring between the quencher and the excited sensor (Santra et

al., 2016). Therefore, the findings from the time-resolved fluorescence tests provide further evidence that the primary mechanism responsible for the quenching of fluorescence is static quenching, which occurs through the formation of a non-emissive ground state complex between sensor **L** and TNP.

Furthermore, it is worth noting that UV-vis absorption investigations conducted on **L** with TNP revealed the emergence of a novel band at around 425 nm accompanied by a level-off tail (Fig.3), further suggesting that charge transfer occurs between them (Gupta et al., 2015). As a matter of fact, dynamic quenching exclusively impacts the excited states of the fluorophore, so it is expected that the absorption spectrum will not change. In contrast, the absorption spectrum of the fluorophore is frequently disrupted due to the formation of ground-state complex (Divya et al., 2022). As a result, the observed disruption in the UV-vis spectrum is fully consistent with the static type of quenching mechanism via charge-transfer complex formation.

In order to further clarify the mechanism for TNP-induced fluorescence quenching, DFT calculations were also carried out. The most energetically-favoured optimized structure of **L** was first determined, and as can be seen in Fig.4, it's frontier molecular orbital diagrams reveal that the majority of the electron density in the HOMO is concentrated within two pyrene molecules. The LUMO can be seen to be localized over the neighboring pyrene. Thus, the intense excimer fluorescence in sensor **L** is most likely driven by the HOMO-LUMO interactions between the ground state and excited state pyrenes (Py-Py*) (Choi et al., 2006). More importantly, the favorable charge-transfer from the sensor **L** to TNP is also understandable from a consideration of the energies of the LUMOs of **L** and the NACs. The LUMO of the electron-rich **L** is at a higher energy than the LUMOs of electron-deficient NACs, allowing transfer of the excited state electron from the LUMO of **L** to the LUMOs of NACs (Fig.5). The lower LUMO energy levels reflect the relative ease with which excited electrons can be transported from the higher-energy LUMO of L to the lower-energy LUMO

of NACs during the quenching process (Dinda et al., 2014). Particularly, the LUMO energy of TNP is the lowest of all the NACs studied, making it the most potent electron acceptor in its excited state. Thus, the maximum fluorescence quenching for TNP is due to more facile electron transfer from sensor **L** to TNP compared to other NACs. Nevertheless, there is a discrepancy between the observed order of quenching efficiency and the LUMO energies of the other NACs. This observation suggests that the charge transfer process alone is not the exclusive mechanism responsible for the remarkably selective fluorescence quenching observed towards TNP. Apart from the transfer of charge, the relocation of energy among fluorophore and NACs may lead to the quenching of fluorescence. Such transfer of energy are widely known as the inner filter effect (IFE) and resonance energy transfer (RET) (Gunture et al., 2022; Wang et al., 2020b).

As depicted in Fig.6a, the absorption spectrum of TNP has a broad range spanning from 280 to 480 nm. The observed spectrum demonstrates substantial overlap with the emission and excitation spectrum of sensor **L**, thereby establishing the necessary conditions for RET and IFE to occur. In general, IFE happens when there is a significant spectral overlap of absorption spectra of the quencher with excitation and/or emission spectra of the fluorophore. On the other hand, in the context of RET, the spectral overlap exclusively arises from the absorption spectra of the quencher and the emission spectra of the fluorophore (Tanwar et al., 2018). In addition, the fluorescence lifetime of the fluorophore is constant during IFE, while the fluorescence lifetime reduces for RET. The aforementioned insignificant change in the fluorescence lifetime (Fig.S13) provides confirmation that the quenching seen is of a static nature, hence ruling out the occurrence of any RET which falls into the classification of dynamic quenching (Goswami et al., 2023; Cui et al., 2023). Therefore, IFE may serve as the primary mechanism accountable for the fluorescence quenching of sensor **L** induced by TNP. This can be explained by the ineffective overlap between the excitation/emission spectra of **L** and the absorption spectra of other NACs, which leads to low IFE efficiency (Fig.6b). The

efficiency of IFE is dependent on the spectral overlap extent, thus, the selectivity toward TNP could also be explained by the IEF mechanism.

To corroborate the interaction between **L** and TNP, a ^{1}H-NMR spectroscopic titration of **L** with TNP was conducted. As shown in Fig.7, the addition of 50 equivalents of TNP resulted in obvious downfield shifts for the peaks of **L** corresponding to the triazole, triazole–*CH*$_2$–pyrene and O–*CH*$_2$–triazole protons by $\Delta\delta$ = 0.14, 0.11 and 0.07 ppm, respectively (Table S2). The downfield shift of the triazole and the adjacent methylene protons after complexation is consistent with the loss of electron density of the triazole groups upon coordination with TNP. Furthermore, significant downfield shifts and extensive broadening are also observed for the peaks assigned to the TNP phenolic protons. To better understand how **L** interacts with TNP, DFT calculations were performed. The gas phase DFT calculations for **L** with TNP were simplified and sped up by focusing solely on a 1:1 complex which is also supported by a Job's plot (Fig.S14). The most stable optimized structures of **L** and TNP were used to generate three possible 1:1 (**L**:TNP) complexes (Fig.S15). The most energetically-favoured optimized structure for the complex is one in which the TNP is "sandwiched" between two pyrene groups through π-π stacking, with the orientation of the hydroxyl and both *ortho* nitro groups strongly directed toward the interior of the host (Fig.8). It can also be seen that hydrogen bonding exists between the phenolic hydroxyl and the N2 nitrogen of the middle triazole with an interatomic distance of 1.997 Å. The optimized structure of the putative complex had a computed interaction energy of -132.93 kJ mol^{-1} which was energetically-favoured by greater than 24 kJ mol^{-1} over the next best optimized 1:1 host:guest complex (Fig.S16). With increasing numbers of TNP molecules, molecular mechanics modeling suggests that the TNP molecules associate more strongly and closer to one another. This can explain the relatively much larger chemical shift changes seen for the hydroxyl groups ($\Delta\delta$ = 1.5 ppm) compared to the other shifts noted above in the ^{1}H-NMR titration. On the other hand, protonation of the nitrogen atom(s) of the triazole(s) by the

strong-acid TNP results in making the triazole ring(s) cationic and electron-deficient and hence can also result in similar downfield shifts of the triazole protons as noted in the ^{1}H-NMR titration and as is also likely in the fluorescence quenching seen in the mixed acetonitrile-HEPES solvent. Particularly, an analogous protonation by TNP with a pyrazoline nanoparticle fluorescent sensor was proposed by Ahmed and co-workers (Ahmed et al., 2017). It is noteworthy also that the chemical shifts of the axial protons in the Ar–CH_2–O methylene bridges, which are related to the conformation of hexahomotrioxacalix[3]arene, were shifted to lower magnetic field (from 3.93 to 4.08 ppm) as also were the equatorial protons and the methylene protons of ArO–CH_2 shifted downfield although less so. The pyrene aromatic protons also displayed different downfield or upfield shifts (Fig.S17). These findings provide additional evidence suggesting that the hexahomotrioxacalix[3]arene undergoes a conformational change when it coordinates with TNP. Previous reports have demonstrated that the flexible hexahomotrioxacalix[3]arene framework possesses the capability to modulate its conformation in order to effectively bind with a specific target (Carpentier et al., 2022; Miranda et al., 2022; Lambert et al., 2020; Teixeira et al., 2020).

3.4 Practical application

Based on the remarkable sensitivity and selectivity of sensor **L** for TNP detection, the standard spike/recovery method was employed to conduct spectrofluorimetric detection of TNP in real water and soil samples. As shown in Table 1, the recoveries of the samples varied from 97.14% to 103.20%, indicating that the proposed method has wonderful practicability. In addition, the RSD (relative standard deviation) of each sample was below 1.28%, revealing the high reproducibility and precision of this approach. To check the reliability of such a spectrofluorimetric approach, HPLC experiments were also conducted on the same samples. The results obtained from the HPLC analysis show a high level of concordance with the spectrofluorimetric approach that was provided. This indicates that the current method is accurate for determining TNP in real samples.

In order to conduct a more comprehensive examination of the potential uses of sensor **L**, the development of low-cost and portable fluorescent test strips was performed. These test strips were specifically designed for the purpose of detecting TNP in real-time at the location of interest. As depicted in Fig.9, the blank test strip exhibited a prominent blue fluorescence upon irradiation with a 365 nm UV lamp. When the test strips were immersed in an aqueous solution of TNP, a noticeable phenomena of fluorescence quenching was observed. An evident disparity in the extent of quenching appeared as the concentration of TNP increased. Additionally, the contact-mode response of the strips to TNP was examined by covering a test strip with TNP crystals for one minute; this produced black spots when illuminated with a UV lamp (Fig.10). In particular, the test strips were successfully used to identify TNP vapor as well as in real water samples. These results demonstrate that the sensor **L** has outstanding sensing performance toward TNP, which served as a convenient and efficient test kit for the instant visualization of TNP.

4 Conclusions

In conclusion, a C_3-symmetrical pyrenyl-triazole functionalized hexahomotrioxacalix[3]arene **L** has been developed as a novel TNP-selective fluorometric and colorimetric sensor. The high sensitivity of sensor **L** toward TNP is achieved by the combination of ground-state charge-transfer complex formation and the inner filter effect. ^{1}H-NMR spectroscopic titrations confirmed that the preorganized 1,2,3-triazole played a crucial role as the hydrogen-bonding motif for bonding with TNP. Moreover, fluorescent test strips based on **L** were fabricated for practical applications in the detection of TNP in real samples. This work presented herein demonstrates the potential of a click-chemically derived triazole-functionalized hexahomotrioxacalix[3]arene for the design of high-efficiency fluorescent sensors for the hazardous trinitrophenol pollutant.

Acknowledgements

We would like to thank the National Natural Science Foundation of China (81903799), Guizhou Provincial Key Technology R&D Program [2020]4Y107, the OTEC at Saga University, and the Cooperative Research Program of "Network Joint Research Center for Materials and Devices (Institute for Materials Chemistry and Engineering, Kyushu University)". The authors extend their appreciation to the Deputyship for Research & Innovation, "Ministry of Education" in Saudi Arabia for funding this research work through project no. (IFKSUOR3-303-2). P.E.G. and S.R. gratefully appreciate the computational resources provided by Acenet and the Digital Research Alliance of Canada.

Appendix A. Supplementary data

References

Ahmed, M., Hameed, S., Ihsan, A., Naseer, M.M., 2017. Fluorescent thiazol-substituted pyrazoline nanoparticles for sensitive and highly selective sensing of explosive 2,4,6-trinitrophenol in aqueous medium, Sens. Actuators B 248, 57–62.

Ahmed, F., Xiong, H., 2021. Recent developments in 1,2,3-triazole-based chemosensors. Dyes Pigm. 185, 108905.

Bener, M., Şen, F.B., Apak, R., 2022. Protamine gold nanoclusters–based fluorescence turn-on sensor for rapid determination of Trinitrotoluene (TNT). Spectrochim. Acta A 279, 121462.

Bryant, J.J., Bunz, U.H.F., 2013. Click to bind: Metal sensors. Chem. Asian J. 8, 1354–1367.

Carpentier, R., Lambert, S., Brunetti, E., Jabin, I., Bartik, K., 2022. Specifc binding of primary ammoniums in aqueous media by homooxacalixarenes incorporated into micelles, J. Org. Chem. 87, 12749–12758.

Choi, J.K., Lee, A., Kim, S., Ham, S., No, K., Kim, J.S., 2006. Fluorescent ratiometry of tetrahomodioxacalix[4]arene pyrenylamides upon cation complexation. Org. Lett. 8, 1601–1604.

Cui, Q., Guo, X., Zhang, W., Dong, W., Duan, Q., 2023. Preparation of porous organic polymer nanoparticles in miniemulsion for 2,4,6-trinitrophenol sensing. Dyes Pigm. 208, 110843.

Dinda, D., Gupta, A., Shaw, B.K., Sadhu, S., Saha, S.K., 2014. Highly selective detection of trinitrophenol by luminescent functionalized reduced graphene oxide through FRET mechanism. ACS Appl. Mater. Interfaces 6, 10722–10728.

Divya, K.M., Savitha, D.P., Krishna, G.A., Dhanya, T.M., Mohanan, P.V., 2022. A thiophene based pyrrolo [1,2-a] quinoxaline fluorescent probe as a “turn-off” sensor for the selective nanomolar detection of sodium ion. J. Photochem. Photobiol. A 431, 114046.

Gledhill, M., Beck, A.J., Stamer, B., Schlosser, C., Achterberg, E.P., 2019. Quantification of munition compounds in the marine environment by solid phase extraction–ultra high performance liquid chromatography with detection by electrospray ionization–mass spectrometry. Talanta 200, 366–372.

Goel, A., Malhotra, R., 2022. Efficient detection of Picric acid by pyranone based Schiff base as a chemosensor. J. Mol. Struct. 1249, 131619.

Gole, B., Shanmugaraju, S., Bara, A.K., Mukherjee, P.S., 2011. Supramolecular polymer for explosives sensing: role of H-bonding in enhancement of sensitivity in the solid state. Chem. Commun. 47, 10046–10048.

Goswami, K.J., Sultana, N., Sarma, N.S., 2023. Duel phase selective inner filter effect-based luminescent sensing for the detection of para-nitrophenol and picric acid. Sens. Actuators B 374, 132778.

Gunture, K., Garg, A.K., Aggarwal, R., Kaushik, J., Prajapati, R.K., Sonkar, S.K., 2022. Non-aqueous onion like nano-carbons from waste diesel-soot used as FRET-based sensor for sensing of nitro-phenols. Environ. Res. 212, 113308.

Gupta, A., Kang, Y.-A., Choi, M.-S., Park, J.S., 2015. Characteristic response of tetra(methylbenzyloxy)-substituted zinc-phthalocyanine toward picric acid. Sens. Actuators B 209, 225–229.

Harathi, J., Thenmozhi, K., 2022. Water-soluble ionic liquid as a fluorescent probe towards distinct binding and detection of 2,4,6-trinitrotoluene and 2,4,6-trinitrophenol in aqueous medium. Chemosphere 286, 131825.

Hu, J.-H., Zhang, W., Ren, C.-X., Xiong, Y., Zhang, J.-Y., He, J., Huang, Y., Tao, Z., Xiao, X., 2023. A novel portable smart phone sensing platform based on a supramolecular fluorescence probe for quick visual quantitative detection of picric acid. Anal. Chim. Acta 1254, 341095.

Ilyas, Q., Waseem, M.T., Junaid, H.M., Khan, Z.A., Munir, F., Shaikh, A.J., Shahzad, S.A., 2022. Fluorescein based fluorescent and colorimetric sensors for sensitive detection of TNP explosive in aqueous medium: Application of logic gate. Spectrochim. Acta A 272, 120994.

Kaur, M., Yusuf, M., Tsang, Y.F., Kim, K.-H., Malik, A.K., 2023. Amine/hydrazone functionalized Cd(II)/Zn(II) metal-organic framework for ultrafast sensitive detection of hazardous 2,4,6-trinitrophenol in water. Sci. Total Environ. 857, 159385.

Kayhomayun, Z., Ghani, K., Zargoosh, K., 2022. Synthesis of samarium orthoferrite-based perovskite nanoparticles as a turn-on fluorescent probe for trace level detection of picric acid. Spectrochim. Acta A 281, 121627.

Kostarev, V.A., Kotkovskii, G.E., Chistyakov, A.A., Akmalov, A.E., 2022. Detection of explosives in vapor phase by field asymmetric ion mobility spectrometry with dopant-assisted laser ionization. Talanta 245, 123414.

Kumar, A., Nath, P., Kumar, V., Tailor, N.K., Satapathi, S., 2023. 3D printed optical sensor for highly sensitive detection of picric acid using perovskite nanocrystals and mechanism of photo-electron transfer. Spectrochim. Acta A 286, 121956.

Lambert, S., Bartik, K., Jabin, I., 2020. Specific binding of primary ammonium ions and lysine-containing peptides in protic solvents by hexahomotrioxacalix[3]arenes. J. Org. Chem. 85, 10062–10071.

Lau, Y.H., Rutledge, P.J., Watkinson, M., Todd, M.H., 2011. Chemical sensors that incorporate click-derived triazoles. Chem. Soc. Rev. 40, 2848–2866.

Liu, Y., Sun, Q., Zhou, H., Gao, H., Li, D., Li, Y., 2022a. One-dimensional Europium-coordination polymer as luminescent sensor for highly selective and sensitive detection of 2,4,6-trinitrophenol. Spectrochim. Acta A 264, 120303.

Liu, X., Han, Y., Shu, Y., Wang, J., Qiu, H., 2022b. Fabrication and application of 2,4,6-trinitrophenol sensors based on fluorescent functional materials. J. Hazard. Mater. 425, 127987.

Miranda, A.S., Marcos, P.M., Ascenso, J.R., Berberan-Santos, M.N., Menezes, F., 2022. Anion binding by fluorescent ureido-hexahomotrioxacalix[3]arene receptors: An NMR, absorption and emission spectroscopic study. Molecules 27, 3247.

Mukherjee, D., Das, P., Kundu, S., Mandal, B., 2022, Engineering of graphene quantum dots by varying the properties of graphene oxide for fluorescence detection of picric acid. Chemosphere 300, 134432.

Nguyen, C.H.T., Nguyen, T.H., Nguyen, T.P.L., Tran, H.L., Luu, T.H., Tran, C.D., Nguyen, Q.-T., Nguyen, L.-T.T., Yokozawa, T., Nguyen, H.T., 2023. Aerobic direct arylation polycondensation of N-perylenyl phenoxazine-based fluorescent conjugated polymers for highly sensitive and selective TNT explosives detection. Dyes Pigm. 219, 111613.

Ni, X.L., Tahara, J., Rahman, S., Zeng, X., Hughes, D.L., Redshaw, C., Yamato, T., 2012. Ditopic receptors based on lower- and upper-rim substituted hexahomotrioxacalix[3]arenes: cation-controlled hydrogen bonding of anion. Chem. Asian J. 7, 519–527.

Park, S.Y., Yoon, J.H., Hong, C.S., Souane, R., Kim, J.S., Matthews, S.E., Vicens, J., 2008. A pyrenyl-appended triazole-based calix[4]arene as a fluorescent sensor for Cd^{2+} and Zn^{2+}. J. Org. Chem. 73, 8212–8218.

Qu, B., Mu, Z., Liu, Y., Liu, Y., Yan, R., Sun, J., Zhang, Z., Li, P., Jing, L., 2020. The synthesis of porous ultrathin graphitic carbon nitride for the ultrasensitive fluorescence detection of 2,4,6-trinitrophenol in environmental water. Environ. Sci.-Nano 7, 262–271.

Santra, D.C., Bera, M.K., Sukul, P.K., Malik, S., 2016. Charge-transfer-induced fluorescence quenching of anthracene derivatives and selective detection of picric acid. Chem. Eur. J. 22, 2012–2019.

Sun, X., Wang, Y., Lei, Y., 2015. Fluorescence based explosive detection: from mechanisms to sensory materials. Chem. Soc. Rev. 44, 8019–8061.

Tanwar, A.S., Adil, L.R., Afroz, M.A., Iyer, P.K., 2018. Inner filter effect and resonance energy transfer based attogram level detection of nitroexplosive picric acid using dual emitting cationic conjugated polyfluorene. ACS Sens. 3, 1451−1461.

Teixeira, F.A., Ascenso, J.R., Cragg, P.J., Hickey, N., Geremia, S., Marcos, P.M., 2020. Recognition of anions, monoamine neurotransmitter and trace amine hydrochlorides by ureido-hexahomotrioxacalix[3]arene ditopic receptors. Eur. J. Org. Chem. 13, 1930–1940.

Thippeswamy, M.S., Naik, L., Maridevarmath, C.V., Savanur, H.M., Malimath, G.H., 2022. Studies on the characterisation of thiophene substituted 1,3,4-oxadiazole derivative for the highly selective and sensitive detection of picric acid. J. Mol. Struct. 1264, 133274.

Wang, J., Yang, Y., Sun, G., Zheng, M., Xie, Z., 2019. A convenient and universal platform for sensing environmental nitro-aromatic explosives based on amphiphilic carbon dots. Environ. Res. 177, 108621.

Wang, B.-W., Jiang, K., Li, J.-X., Luo, S.-H., Wang, Z.-Y., Jiang, H.-F., 2020a. 1,1-Diphenylvinylsulfide as a functional AIEgen derived from the aggregation-caused-quenching molecule 1,1-diphenylethene through simple thioetherification. Angew. Chem. Int. Ed. 59, 2338–2343.

Wang, X., Liu, Y., Zhou, Q., Sheng, X., Sun, Y., Zhou, B., Zhao, J., Guo, J., 2020b. A reliable and facile fluorescent sensor from carbon dots for sensing 2,4,6-trinitrophenol based on inner filter effect. Sci. Total Environ. 720, 137680.

Wang, T., Zheng, Q., Zhu, A., Wang, Y., Guo, X., Liu, X., Ying, Y., Wu, Y., Wen, Y., Yang, H., 2022. Construction of Jaffe reaction-based SERS chip for determination of trace picric acid. Sens. Actuators B 368, 132201.

Weiss, J.M., McKay, A.J., DeRito, C., Watanabe, C., Thorn, K.A., Madsen, E.L., 2004. Development and application of pyrolysis gas chromatography/mass spectrometry for the analysis of bound trinitrotoluene residues in soil. Environ. Sci. Technol. 38, 2167–2174.

Wu, C., Wang, C.-Z., Zhu, Q., Zeng, X., Redshaw, C., Yamato, T., 2018. Click synthesis of a quinoline-functionalized hexahomotrioxacalix[3]arene: A turn-on fluorescence chemosensor for Fe^{3+}. Sens. Actuators B 254, 52–58.

Wu, C., Rahman, S., Jiang, X.-K., Wang, C.-Z., Alodhayb, A., Alibrahim, K.A., Georghiou, P.E., Yamato, T., 2023. A fluorescent receptor for alkylammonium ions based on an anthryl-linked triazole-modified hexahomotrioxacalix[3]arene. J. Mol. Struct. 1286, 135615.

Xie, H.-F., Wu, C., Zou, J., Yang, Y.-X., Xu, H., Zhang, Q.-L., Redshaw, C., Yamato, T., 2020. A pyrenyl-appended C_{3v}-symmetric hexahomotrioxacalix[3]arene for selective fluorescence sensing of iodide. Dyes Pigm. 178, 108340.

Zan, Y., Kang, Y., Wang, B., Cui, S., Shen, Z., Shu, J., Kong, X., Chen, L., Yan, X., Li, Y., 2022. Amphiphilic fluorescent nanospheres for quantitative sensing of trinitrophenol in water system. Dyes Pigm. 202, 110296.

Zheng, C., Ling, Y., Chen, J., Yuan, X., Li, S., Zhang, Z., 2023. Design of a versatile and selective electrochemical sensor based on dummy molecularly imprinted PEDOT/laser-induced graphene for nitroaromatic explosives detection. Environ. Res. 236, 116769.

Zhu, P., Lin, L., Chen, W., Liu, L., 2022. Ionic modification on COF with rare earth ions for the selective optical sensing and removal of picronitric acid. Chemosphere 302, 134785.

Graphical Abstract

A facile and sensitive hexahomotrioxacalix[3]arene-based fluorescent sensor for the detection of trace amounts of 2,4,6-trinitrophenol

A C_3-symmetrical pyrenyl-triazole functionalized hexahomotrioxacalix[3]arene have been developed as a novel TNP-selective fluorescent sensor.

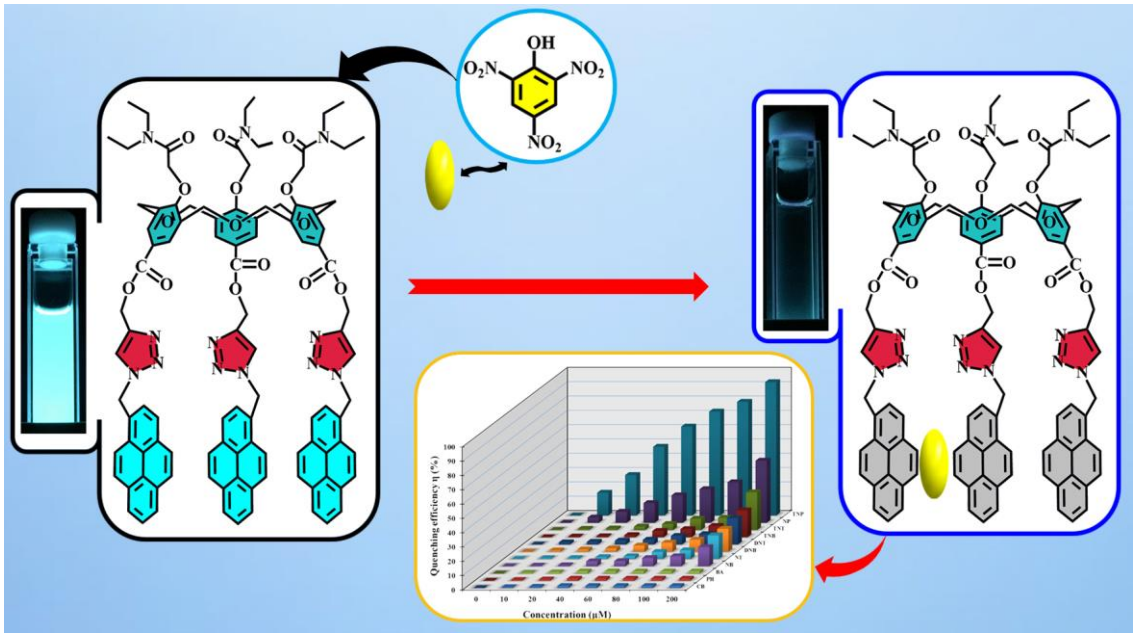

HIGHLIGHTS

- A facile and sensitive fluorescent sensor was constructed for sensing of TNP based on hexahomotrioxacalix[3]arene.
- The present spectrofluorimetric method is extremely sensitive and selective for TNP detection.
- The inner filter effect and charge-transfer complex dominated the sensing mechanism.
- Test strips were fabricated to facilitate the visual detection of TNP.

A facile and sensitive hexahomotrioxacalix[3]arene-based fluorescent sensor for the detection of trace amounts of 2,4,6-trinitrophenol

Abstract:

Nitroaromatic compounds are common explosives and toxic pollutants, the selective and sensitive detection of which is of great importance. Herein, a facile and sensitive fluorescent sensor **L** was constructed for the sensing of TNP based on the hexahomotrioxacalix[3]arene skeleton. The fluorescence emission of **L** was drastically quenched in the presence of 2,4,6-trinitrophenol (TNP), while other tested NACs, metal ions, and anions induced negligible changes. Under the optimized conditions, the spectroscopic studies revealed that **L** exhibited extremely sensitive and selective TNP recognition, with a detection limit of 9.17×10^{-7} M and a quenching constant of 2.44×10^{4} M^{-1}. The sensitivity of sensor **L** for TNP was attributed to the formation of a ground-state charge-transfer complex and an inner filter effect, which also contributed to the special selectivity of the sensor among the various nitroaromatic analogues. Compared with previous reports, **L** can serve as a highly efficient sensor for the sensing of TNP and can be employed over a wide pH range of 2 to 12. Sensor **L** was effectively used to quantify TNP in real water and soil samples. Additionally, fluorescent test strips were also developed for visual and rapid detection of TNP in both the solution and vapour phases.

Keywords: Fluorescent sensor, Hexahomotrioxacalix[3]arene, Click reaction, Trinitrophenol detection.

1 Introduction

Nitroaromatic compounds (NACs) are the major components of explosives. NACs, including TNP, are also common chemical reagents that are extensively used in the wider chemical, pharmaceutical, leather and dye industries (Zan et al., 2022). However, as a result of its widespread use, as well as in explosives, once TNP in particular is released into the environment, due to its high solubility in water, it readily contaminates soil and aquatic systems (Liu et al., 2022a). Furthermore, due to its electron-deficient nature, TNP is difficult to be degraded in both biosystems and the environment, thus becoming one of the major environmental pollutants (Kumar et al., 2023). Significantly, TNP exhibits various toxic effects towards living organisms, such as carcinogenicity, mutagenicity, liver damage, skin irritation, etc (Goel and Malhotra, 2022). Consequently, the United States Environmental Protection Agency (EPA) included TNP in its list of priority pollutants (Ilyas et al., 2022). It is therefore of significant interest and relevance to develop accurate and sensitive analytical methods for the selective detection of TNP.

To date, many analytical techniques have been developed to detect NACs, such as HPLC (Gledhill et al., 2019), GC-MS (Weiss et al., 2004), ion mobility spectroscopy (Kostarev et al., 2022), surface-enhanced Raman spectroscopy (Wang et al., 2022), electrochemistry analysis (Zheng et al., 2023) and fluorescence spectroscopy (Liu et al., 2022b). Among these various methods, fluorescence based sensing methodologies have proven to be excellent candidates by virtue of their excellent selectivity and sensitivity, short response time, real-time monitoring, and operational simplicity (Harathi and Thenmozhi, 2022; Qu et al., 2020). In this regard, fluorescent materials including conjugated polymers (Nguyen et al., 2023), supramolecular ensembles (Hu et al., 2023), MOFs (Kaur et al., 2023), COFs (Zhu et al., 2022), AIEgens (Wang et al., 2020a), small organic molecules (Thippeswamy et al., 2022), nanoparticles (Kayhomayun et al., 2022), nanoclusters (Bener et al., 2022), carbon

dots (Wang et al., 2019), and quantum dots (Mukherjee et al., 2022) have been developed for the detection of NACs.

The click reaction has been extensively employed to synthesize a wide range of 1,2,3-triazole-based fluorescent sensors that have been developed for the sensing of ionic species (Lau et al., 2011; Bryant and Bunz, 2013; Ahmed and Xiong, 2021). Nevertheless, these fluorescence systems have scarcely been specifically designed for the detection of NACs. The 1,2,3-triazole ring possesses three nitrogen atoms and thus, their lone pair electrons can coordinate to metal ions, and can be hydrogen bond and/or proton acceptor(s). On the other hand, NACs commonly function as electron acceptors owing to the electron-withdrawing nature of the nitro group(s) (Gole et al., 2011). As a result, significant noncovalent interactions may be formed between 1,2,3-triazole and NACs. These factors inspired us to design an efficient fluorescent sensor for sensing NACs via the click reaction.

In connection with our ongoing research on sensors for environmentally and biologically important guest species (Wu et al., 2023; Xie et al., 2020; Wu et al., 2018), herein, we report a novel hexahomotrioxacalix[3]arene-based sensor **L** with preorganized triazoles as recognition sites and has pendant pyrenes as the fluorophores for the fluorometric and colorimetric sensing of TNP. The sensing mechanism was systematically investigated by UV-vis/fluorescence titrations, fluorescence lifetime measurements, ^{1}H NMR spectroscopic titration analysis, and DFT caculations. Sensor **L** was successfully employed to detect TNP in actual water and soil samples with satisfactory results. As well, fluorescent test strips were also fabricated for the convenient and cost-effective real-time monitoring of TNP. The findings of this work present an appropriate strategy for the design and fabrication of fluorescent sensors for the rapid identification and quantification of the potentially TNP pollutant.

2 Experimental

2.1 Materials

All reagents were obtained from commercial suppliers and utilised without additional purification. NMR spectra were measured on a Bruker 400 MHz instrument. HRMS spectra were recorded using a mass spectrometer (Agilent 6540 Q-TOF). Fluorescence spectra were performed on a Shimadzu RF-5301PC spectrometer. Quantum yields were measured using absolute method using a Hamamatsu C11347-11 Quantaurus-QY Analyzer. Fluorescence lifetimes were determined on the Edinburgh FLS1000 steady-state transient fluorescence spectrometer. UV-vis spectra were taken on a Shimadzu UV-2600 UV-vis spectrometer. HPLC analysis was carried out on Agilent 1290 II-6460.

2.2 Synthesis and Characterization

The 1-azidomethylpyrene (Park et al., 2008) and precursors **1**, **2** (Ni et al., 2012) were produced according to the reported procedures. A suspension of compound **2** (890 mg, 1.0 mmol) and K_2CO_3 (1.24 g, 9.0 mmol) was heated at reflux for 1 h in dry acetone (80 mL), then propargyl bromide (480 mg, 4.0 mmol) was added, and the reaction mixture was refluxed for 24 h. After that, the reaction was cooled to room temperature, and the filtrate was concentrated. The residue was purified by column chromatography (dichloromethane as eluent) to afford the desired compound **3** (750 mg, 75 %). ^{1}H NMR (400 MHz, $CDCl_3$): δ = 7.58 (s, 6H, ArH_{calix}), 4.87–4.91 (d, 6H, J = 13.2 Hz, Ar$CH_{2(eq)}$O), 4.86 (s, 6H, OCH_2-alkynyl), 4.66 (s, 6H, ArOCH_2), 4.49–4.52 (d, 6H, J = 13.2 Hz, Ar$CH_{2(ax)}$O), 3.28–3.41 (dq, 12H, NCH_2CH$_3$), 2.51 (s, 3H, C≡CH), 1.12–1.21 (dt, 18H, NCH$_2$$CH_3$). ^{13}C NMR (100 MHz, $CDCl_3$) δ = 166.84, 164.72, 159.90, 132.03, 131.86, 125.08, 78.13, 74.72, 72.26, 68.93, 52.19, 41.06, 40.11, 14.32, 12.98. HRMS (FAB$^+$): calcd. for [$C_{54}H_{64}N_3O_{15}$ + H]$^+$ 994.4337; found 994.4335.

A well-stirred solution of Compound **3** (500 mg, 0.50 mmol), 1-azidomethylpyrene (425 mg, 1.65 mmol), and CuI (30 mg) in 50 mL of THF/H_2O (4:1) was refluxed for 24 h. The solvent was removed, and the resulting residue was subsequently purified via column

chromatography (ethyl acetate as eluent) to afford **L** as white solid (600 mg, 68 %). ^{1}H NMR (400 MHz, $CDCl_3$): δ = 8.03–8.05 (d, 3H, *J* = 8.0 Hz, Py-*H*), 7.93–7.95 (d, 3H, *J* = 8.0 Hz, Py-*H*), 7.87–7.89 (d, 3H, *J* = 8.0 Hz, Py-*H*), 7.68–7.81 (m, 21H, Py-*H* (18H) and triazole-*H* (3H); overlapped), 7.12 (s, 6H, ArH_{calix}), 5.96 (s, 6H, triazole-CH_2-Py), 5.18 (s, 6H, OCH_2-triazole), 4.58–4.60 (d, 6H, *J* = 12.8 Hz, Ar$CH_{2(eq)}$O), 4.45 (s, 6H, ArOCH_2), 3.93–3.95 (d, 6H, *J* = 12.8 Hz, Ar$CH_{2(ax)}$O), 3.18–3.34 (dq, 12H, NCH_2CH_3), 1.06–1.12 (q, 18H, NCH_2CH_3). ^{13}C NMR (100 MHz, $CDCl_3$) δ = 166.81, 165.21, 159.96, 143.54, 131.77, 131.70, 131.57, 130.72, 130.13, 128.51, 127.75, 127.40, 126.85, 126.79, 125.88, 125.42, 125.32, 124.71, 124.61, 124.48, 124.36, 123.99, 121.76, 71.96, 68.68, 57.97, 51.94, 40.89, 39.96, 14.21, 12.91. HRMS (FAB^+): calcd. for $[C_{105}H_{96}N_{12}O_{15} + H]^+$ 1766.7230; found 1766.7228.

2.3 UV-vis and fluorescence titrations

Both the sensor **L** and the analytes were prepared as 1 mM stock solutions by dissolving them in acetonitrile. The stock solutions were diluted to the appropriate concentration with acetonitrile and buffer solutions. In titration experiments, a 3 mL solution of **L** was typically added to a quartz cuvette, followed by the addition of various stock solutions of analytes using a micro-syringe. Each titration was replicated three times in order to obtain consistent results.

2.4 Fluorescence sensing of TNP in real samples

Prior to usage, the crude water samples were filtered via a 0.22 μm membrane filter. The pH of the water samples was adjusted to 7.4 with HEPES buffer, and then different amounts of TNP were added. The obtained samples underwent further treatment using **L** and CH_3CN, resulting in the formation of final mixtures containing 50% CH_3CN. Subsequently, the fluorescence spectra of the mixes comprising **L** (with a final concentration of 1.0 μM) and TNP were recorded within 30 seconds. For the soil sample analysis, 1 g of soil samples were mixed with 1.0 mg and 2.0 mg of TNP, respectively, and subsequently dissolved in 100 mL deionized water. The soil samples were then filtered through a 0.22 μm membrane filter after

being ultrasonically treated for 15 minutes. Then, the fluorescence was measured after the stock solution of **L** (with a final concentration of 1.0 μM) was introduced.

2.5 HPLC analysis

For HPLC analysis, the C18 column (250×4.6 mm^2 id, 5 μm) was used as a stationary phase and 357 nm was chosen as detection wavelength. The mobile phase consisted of a mixture of methanol and 0.2% acetic acid in a 50:50 ratio. The temperature of the column was kept at 40 °C.

2.6 Fluorescent Test Strips

Fluorescent test strips were fabricated through the immersion of filter paper into the dichloromethane solution of **L**, followed by subsequent air drying. The detection method involved immersing the test papers into an aqueous solution of TNP, followed by drying and then observation under a 365 nm UV light.

3 Results and discussion

3.1 Synthesis

The synthetic pathway of sensor **L** is outlined in Scheme 1. The calixarene skeleton was fixed in the *cone* conformation by first introducing N,N-diethylamide by O-alkylation of the hydroxyl groups located at the lower-rim of the hexahomotrioxacalix[3]arene **1**. Subsequent base hydrolysis of the upper-rim ester yielded the corresponding triacid derivative **2**, and the intermediate **3** was successfully synthesized by employing propargyl bromide in the presence of K_2CO_3 as base. Submitting 1-azidomethylpyrene to a Cu(I)-catalyzed 1,3-dipolar cycloaddition reaction with compound **3** at click conditions resulted in a 68% yield of the sensor **L**. All chemicals synthesised in this study were completely characterised by ^{1}H and ^{13}C NMR spectroscopy, and HRMS (Fig.S1–S3).

3.2 Luminescent properties and detection of TNP

In order to obtain the optimal conditions for analytical applications, the fluorescence characteristics of compound **L** were examined in various solvent mixtures. As shown in Fig.S4, **L** emitted much stronger fluorescence in the CH_3CN/H_2O mixed solvents. In addition, the emission spectra of **L** were recorded by introducing varying water fractions (f_w) into the CH_3CN solution. As can be seen from Fig.S5, the fluorescence intensity enhanced gradually when f_w increases from 0% to 60%. However, a significant fluorescence decrease can be observed when the water content exceeds 70%. Subsequently, an assessment was conducted to examine the impact of pH on the fluorescence signals of **L**. This was achieved by altering the pH values within the range of 2.0 to 12.0. Fluorescence signals exhibited little variation with alteration of pH throughout the range of 5.0 to 12.0 (Fig.S6). Based on the above experimental findings, the CH_3CN/HEPES (v/v, 1:1, pH=7.4) system was applied in the experiments that followed.

The photophysical properties of **L** were studied by the absorption and fluorescence spectra in a 1:1 CH_3CN/HEPES pH=7.4 mixed solvent system (Fig.S7). The UV-vis absorption spectrum of **L** shows two absorption peaks characteristic of pyrene at 328 nm and 343 nm. The most intense absorption maximum (λ_{abs}) was observed at 343 nm, and the molar absorption coefficient (ε) was 8.58×10^4 L mol^{-1} cm^{-1}. Upon excitation at 343 nm, the emission spectra of **L** exhibits a prominent excimer emission at 484 nm arising from the intramolecular π-stacked pyrene units, with a quantum yield (φ) of 0.22. To evaluate the sensing ability of the designed receptor **L** in detecting NACs, we conducted preliminary fluorescence titration studies against TNP. The excimer emissions were efficiently quenched upon the incremental addition of TNP, and the shapes of the emission spectra did not significantly change (Fig.1). Meanwhile, the quenching in the fluorescence emission could be readily observed when illuminated with a UV lamp at 365 nm. To compare the sensing

selectivity of **L** toward TNP, fluorescence titration experiments using **L** were also performed with other NACs and potential interferents, including metal ions and anions. The results presented in Fig.2 and Fig.S8 demonstrate that the relative quenching efficiencies of different analytes towards sensor **L** are barely affected, implying that **L** may be potentially usable for TNP detection in actual samples. Among the tested analytes, it is worth noting that only TNP demonstrated a significant quenching efficiency, and the initial fluorescence intensity of **L** decreased by 93.2% when only 200 μM TNP was added. The calibration curve obtained for TNP exhibits clear linearity within the concentration range of 0 to 50 μM. Thus, the given TNP determination method achieved a detection limit of 9.17×10^{-7} M and a quantitation limit of 3.06×10^{-6} M, especially the precision (RSD%) was found to be 0.33% (Fig.S9). Significantly, the degree of emission quenching observed at the 10-second interval was nearly identical to that observed after a 24-hour period (Fig.S10), confirming the fast response and the stability of present system. This system therefore represents a fluorescent sensor that can be used to determine the concentration of TNP quantitatively.

Subsequently, UV-vis absorption titration experiments were also investigated to assess whether **L** could serve as a colorimetric sensor for TNP. As depicted in Figure 3, a notable increase in the initial absorption intensity was observed when TNP was gradually introduced into the solution of **L**. In the meanwhile, it was observed that the solution underwent a distinct and readily observable alteration in hue, transitioning from a state of transparency to a reddish orange appearance (Fig.3, inset). A linear correlation was observed between the concentration of TNP and the absorption intensity over the range of 0 to 160 μM (Fig.S11). This means that in addition to its use as a fluorescence sensor, **L** can also be a reliable colorimetric sensor for the detection of TNP at low concentrations. Significantly, in terms of selectivity, sensitivity, and limit of detection, **L** acts as a more sensitive TNP sensor than many other sensors that have been described thus far (Table S1).

3.3 The mechanism for the sensing of TNP with L

To better understand the quenching behavior exhibited by sensor **L** when exposed to TNP, the quenching mechanism needs to be well corroborated. Quenching can manifest through multiple mechanisms, typically categorised as static quenching and dynamic quenching. By using the Stern-Volmer equation ($I_0/I = 1 + K_{SV}[Q]$) to fit the observed data, we were able to get insight into the specifics of the quenching process in **L**. As depicted in Fig.S12, the Stern-Volmer plot exhibits a linear trend at low concentrations (up to 50 μM) and a non-linear upward curving at higher quencher concentrations. The linear regression analysis of the plot obtained at lower concentrations yielded a quenching constant of 2.44×10^4 M^{-1} for TNP. This result suggests that sensor **L** has a considerable quenching effect on TNP. Generally, a linear Stern–Volmer plot represents a singular (static or dynamic) quenching mechanism, whereas a positive deviation from linearity suggests the existence of a combined quenching process involving both static and dynamic mechanisms (Sun et al., 2015). The nature of Stern–Volmer plot in the present system falls into the latter category, indicating that a combination of quenching processes contribute to the emission quenching. In order to clarify which factor is the dominant one, time-resolved fluorescence measurements were conducted in the absence and presence of TNP. The lifetime decay plot of **L**, as depicted in Fig.S13, demonstrated that the introduction of TNP in a sequential manner resulted in negligible changes to the fluorescence lifetime. The average lifetime value (τ) of **L** at 484 nm (λ_{ex} = 343 nm) was found to be 141.45 ± 0.22 ns, further addition of 25 and 50 equivalents of TNP into the solution of **L** gave lifetime values of 140.89 ± 0.14 and 140.54 ± 0.18 ns, respectively. In the static mechanism, it can be observed that the fluorescence lifetime remains unaffected. This is due to the binding of the quencher with the sensor in its ground state, resulting in the formation of a non-fluorescent complex or "dark state" with the quencher. Consequently, the molecules that are not bound exhibit their inherent lifetimes. In contrast, the fluorescence lifespan of the dynamic mechanism is expected to decrease as a result of diffusive collisions occurring between the quencher and the excited sensor (Santra et

al., 2016). Therefore, the findings from the time-resolved fluorescence tests provide further evidence that the primary mechanism responsible for the quenching of fluorescence is static quenching, which occurs through the formation of a non-emissive ground state complex between sensor **L** and TNP.

Furthermore, it is worth noting that UV-vis absorption investigations conducted on **L** with TNP revealed the emergence of a novel band at around 425 nm accompanied by a level-off tail (Fig.3), further suggesting that charge transfer occurs between them (Gupta et al., 2015). As a matter of fact, dynamic quenching exclusively impacts the excited states of the fluorophore, so it is expected that the absorption spectrum will not change. In contrast, the absorption spectrum of the fluorophore is frequently disrupted due to the formation of ground-state complex (Divya et al., 2022). As a result, the observed disruption in the UV-vis spectrum is fully consistent with the static type of quenching mechanism via charge-transfer complex formation.

In order to further clarify the mechanism for TNP-induced fluorescence quenching, DFT calculations were also carried out. The most energetically-favoured optimized structure of **L** was first determined, and as can be seen in Fig.4, it's frontier molecular orbital diagrams reveal that the majority of the electron density in the HOMO is concentrated within two pyrene molecules. The LUMO can be seen to be localized over the neighboring pyrene. Thus, the intense excimer fluorescence in sensor **L** is most likely driven by the HOMO-LUMO interactions between the ground state and excited state pyrenes (Py-Py*) (Choi et al., 2006). More importantly, the favorable charge-transfer from the sensor **L** to TNP is also understandable from a consideration of the energies of the LUMOs of **L** and the NACs. The LUMO of the electron-rich **L** is at a higher energy than the LUMOs of electron-deficient NACs, allowing transfer of the excited state electron from the LUMO of **L** to the LUMOs of NACs (Fig.5). The lower LUMO energy levels reflect the relative ease with which excited electrons can be transported from the higher-energy LUMO of L to the lower-energy LUMO

of NACs during the quenching process (Dinda et al., 2014). Particularly, the LUMO energy of TNP is the lowest of all the NACs studied, making it the most potent electron acceptor in its excited state. Thus, the maximum fluorescence quenching for TNP is due to more facile electron transfer from sensor **L** to TNP compared to other NACs. Nevertheless, there is a discrepancy between the observed order of quenching efficiency and the LUMO energies of the other NACs. This observation suggests that the charge transfer process alone is not the exclusive mechanism responsible for the remarkably selective fluorescence quenching observed towards TNP. Apart from the transfer of charge, the relocation of energy among fluorophore and NACs may lead to the quenching of fluorescence. Such transfer of energy are widely known as the inner filter effect (IFE) and resonance energy transfer (RET) (Gunture et al., 2022; Wang et al., 2020b).

As depicted in Fig.6a, the absorption spectrum of TNP has a broad range spanning from 280 to 480 nm. The observed spectrum demonstrates substantial overlap with the emission and excitation spectrum of sensor **L**, thereby establishing the necessary conditions for RET and IFE to occur. In general, IFE happens when there is a significant spectral overlap of absorption spectra of the quencher with excitation and/or emission spectra of the fluorophore. On the other hand, in the context of RET, the spectral overlap exclusively arises from the absorption spectra of the quencher and the emission spectra of the fluorophore (Tanwar et al., 2018). In addition, the fluorescence lifetime of the fluorophore is constant during IFE, while the fluorescence lifetime reduces for RET. The aforementioned insignificant change in the fluorescence lifetime (Fig.S13) provides confirmation that the quenching seen is of a static nature, hence ruling out the occurrence of any RET which falls into the classification of dynamic quenching (Goswami et al., 2023; Cui et al., 2023). Therefore, IFE may serve as the primary mechanism accountable for the fluorescence quenching of sensor **L** induced by TNP. This can be explained by the ineffective overlap between the excitation/emission spectra of **L** and the absorption spectra of other NACs, which leads to low IFE efficiency (Fig.6b). The

efficiency of IFE is dependent on the spectral overlap extent, thus, the selectivity toward TNP could also be explained by the IEF mechanism.

To corroborate the interaction between **L** and TNP, a ^{1}H-NMR spectroscopic titration of **L** with TNP was conducted. As shown in Fig.7, the addition of 50 equivalents of TNP resulted in obvious downfield shifts for the peaks of **L** corresponding to the triazole, triazole–*CH*$_2$–pyrene and O–*CH*$_2$–triazole protons by $\Delta\delta$ = 0.14, 0.11 and 0.07 ppm, respectively (Table S2). The downfield shift of the triazole and the adjacent methylene protons after complexation is consistent with the loss of electron density of the triazole groups upon coordination with TNP. Furthermore, significant downfield shifts and extensive broadening are also observed for the peaks assigned to the TNP phenolic protons. To better understand how **L** interacts with TNP, DFT calculations were performed. The gas phase DFT calculations for **L** with TNP were simplified and sped up by focusing solely on a 1:1 complex which is also supported by a Job's plot (Fig.S14). The most stable optimized structures of **L** and TNP were used to generate three possible 1:1 (**L**:TNP) complexes (Fig.S15). The most energetically-favoured optimized structure for the complex is one in which the TNP is "sandwiched" between two pyrene groups through π-π stacking, with the orientation of the hydroxyl and both *ortho* nitro groups strongly directed toward the interior of the host (Fig.8). It can also be seen that hydrogen bonding exists between the phenolic hydroxyl and the N2 nitrogen of the middle triazole with an interatomic distance of 1.997 Å. The optimized structure of the putative complex had a computed interaction energy of -132.93 kJ mol^{-1} which was energetically-favoured by greater than 24 kJ mol^{-1} over the next best optimized 1:1 host:guest complex (Fig.S16). With increasing numbers of TNP molecules, molecular mechanics modeling suggests that the TNP molecules associate more strongly and closer to one another. This can explain the relatively much larger chemical shift changes seen for the hydroxyl groups ($\Delta\delta$ = 1.5 ppm) compared to the other shifts noted above in the ^{1}H-NMR titration. On the other hand, protonation of the nitrogen atom(s) of the triazole(s) by the

strong-acid TNP results in making the triazole ring(s) cationic and electron-deficient and hence can also result in similar downfield shifts of the triazole protons as noted in the ^{1}H-NMR titration and as is also likely in the fluorescence quenching seen in the mixed acetonitrile-HEPES solvent. Particularly, an analogous protonation by TNP with a pyrazoline nanoparticle fluorescent sensor was proposed by Ahmed and co-workers (Ahmed et al., 2017). It is noteworthy also that the chemical shifts of the axial protons in the Ar–CH_2–O methylene bridges, which are related to the conformation of hexahomotrioxacalix[3]arene, were shifted to lower magnetic field (from 3.93 to 4.08 ppm) as also were the equatorial protons and the methylene protons of ArO–CH_2 shifted downfield although less so. The pyrene aromatic protons also displayed different downfield or upfield shifts (Fig.S17). These findings provide additional evidence suggesting that the hexahomotrioxacalix[3]arene undergoes a conformational change when it coordinates with TNP. Previous reports have demonstrated that the flexible hexahomotrioxacalix[3]arene framework possesses the capability to modulate its conformation in order to effectively bind with a specific target (Carpentier et al., 2022; Miranda et al., 2022; Lambert et al., 2020; Teixeira et al., 2020).

3.4 Practical application

Based on the remarkable sensitivity and selectivity of sensor **L** for TNP detection, the standard spike/recovery method was employed to conduct spectrofluorimetric detection of TNP in real water and soil samples. As shown in Table 1, the recoveries of the samples varied from 97.14% to 103.20%, indicating that the proposed method has wonderful practicability. In addition, the RSD (relative standard deviation) of each sample was below 1.28%, revealing the high reproducibility and precision of this approach. To check the reliability of such a spectrofluorimetric approach, HPLC experiments were also conducted on the same samples. The results obtained from the HPLC analysis show a high level of concordance with the spectrofluorimetric approach that was provided. This indicates that the current method is accurate for determining TNP in real samples.

In order to conduct a more comprehensive examination of the potential uses of sensor **L**, the development of low-cost and portable fluorescent test strips was performed. These test strips were specifically designed for the purpose of detecting TNP in real-time at the location of interest. As depicted in Fig.9, the blank test strip exhibited a prominent blue fluorescence upon irradiation with a 365 nm UV lamp. When the test strips were immersed in an aqueous solution of TNP, a noticeable phenomena of fluorescence quenching was observed. An evident disparity in the extent of quenching appeared as the concentration of TNP increased. Additionally, the contact-mode response of the strips to TNP was examined by covering a test strip with TNP crystals for one minute; this produced black spots when illuminated with a UV lamp (Fig.10). In particular, the test strips were successfully used to identify TNP vapor as well as in real water samples. These results demonstrate that the sensor **L** has outstanding sensing performance toward TNP, which served as a convenient and efficient test kit for the instant visualization of TNP.

4 Conclusions

In conclusion, a C_3-symmetrical pyrenyl-triazole functionalized hexahomotrioxacalix[3]arene **L** has been developed as a novel TNP-selective fluorometric and colorimetric sensor. The high sensitivity of sensor **L** toward TNP is achieved by the combination of ground-state charge-transfer complex formation and the inner filter effect. ^{1}H-NMR spectroscopic titrations confirmed that the preorganized 1,2,3-triazole played a crucial role as the hydrogen-bonding motif for bonding with TNP. Moreover, fluorescent test strips based on **L** were fabricated for practical applications in the detection of TNP in real samples. This work presented herein demonstrates the potential of a click-chemically derived triazole-functionalized hexahomotrioxacalix[3]arene for the design of high-efficiency fluorescent sensors for the hazardous trinitrophenol pollutant.

Acknowledgements

We would like to thank the National Natural Science Foundation of China (81903799), Guizhou Provincial Key Technology R&D Program [2020]4Y107, the OTEC at Saga University, and the Cooperative Research Program of "Network Joint Research Center for Materials and Devices (Institute for Materials Chemistry and Engineering, Kyushu University)". The authors extend their appreciation to the Deputyship for Research & Innovation, "Ministry of Education" in Saudi Arabia for funding this research work through project no. (IFKSUOR3-303-2). P.E.G. and S.R. gratefully appreciate the computational resources provided by Acenet and the Digital Research Alliance of Canada.

Appendix A. Supplementary data

References

Ahmed, M., Hameed, S., Ihsan, A., Naseer, M.M., 2017. Fluorescent thiazol-substituted pyrazoline nanoparticles for sensitive and highly selective sensing of explosive 2,4,6-trinitrophenol in aqueous medium, Sens. Actuators B 248, 57–62.

Ahmed, F., Xiong, H., 2021. Recent developments in 1,2,3-triazole-based chemosensors. Dyes Pigm. 185, 108905.

Bener, M., Şen, F.B., Apak, R., 2022. Protamine gold nanoclusters–based fluorescence turn-on sensor for rapid determination of Trinitrotoluene (TNT). Spectrochim. Acta A 279, 121462.

Bryant, J.J., Bunz, U.H.F., 2013. Click to bind: Metal sensors. Chem. Asian J. 8, 1354–1367.

Carpentier, R., Lambert, S., Brunetti, E., Jabin, I., Bartik, K., 2022. Specifc binding of primary ammoniums in aqueous media by homooxacalixarenes incorporated into micelles, J. Org. Chem. 87, 12749–12758.

Choi, J.K., Lee, A., Kim, S., Ham, S., No, K., Kim, J.S., 2006. Fluorescent ratiometry of tetrahomodioxacalix[4]arene pyrenylamides upon cation complexation. Org. Lett. 8, 1601–1604.

Cui, Q., Guo, X., Zhang, W., Dong, W., Duan, Q., 2023. Preparation of porous organic polymer nanoparticles in miniemulsion for 2,4,6-trinitrophenol sensing. Dyes Pigm. 208, 110843.

Dinda, D., Gupta, A., Shaw, B.K., Sadhu, S., Saha, S.K., 2014. Highly selective detection of trinitrophenol by luminescent functionalized reduced graphene oxide through FRET mechanism. ACS Appl. Mater. Interfaces 6, 10722–10728.

Divya, K.M., Savitha, D.P., Krishna, G.A., Dhanya, T.M., Mohanan, P.V., 2022. A thiophene based pyrrolo [1,2-a] quinoxaline fluorescent probe as a “turn-off” sensor for the selective nanomolar detection of sodium ion. J. Photochem. Photobiol. A 431, 114046.

Gledhill, M., Beck, A.J., Stamer, B., Schlosser, C., Achterberg, E.P., 2019. Quantification of munition compounds in the marine environment by solid phase extraction–ultra high performance liquid chromatography with detection by electrospray ionization–mass spectrometry. Talanta 200, 366–372.

Goel, A., Malhotra, R., 2022. Efficient detection of Picric acid by pyranone based Schiff base as a chemosensor. J. Mol. Struct. 1249, 131619.

Gole, B., Shanmugaraju, S., Bara, A.K., Mukherjee, P.S., 2011. Supramolecular polymer for explosives sensing: role of H-bonding in enhancement of sensitivity in the solid state. Chem. Commun. 47, 10046–10048.

Goswami, K.J., Sultana, N., Sarma, N.S., 2023. Duel phase selective inner filter effect-based luminescent sensing for the detection of para-nitrophenol and picric acid. Sens. Actuators B 374, 132778.

Gunture, K., Garg, A.K., Aggarwal, R., Kaushik, J., Prajapati, R.K., Sonkar, S.K., 2022. Non-aqueous onion like nano-carbons from waste diesel-soot used as FRET-based sensor for sensing of nitro-phenols. Environ. Res. 212, 113308.

Gupta, A., Kang, Y.-A., Choi, M.-S., Park, J.S., 2015. Characteristic response of tetra(methylbenzyloxy)-substituted zinc-phthalocyanine toward picric acid. Sens. Actuators B 209, 225–229.

Harathi, J., Thenmozhi, K., 2022. Water-soluble ionic liquid as a fluorescent probe towards distinct binding and detection of 2,4,6-trinitrotoluene and 2,4,6-trinitrophenol in aqueous medium. Chemosphere 286, 131825.

Hu, J.-H., Zhang, W., Ren, C.-X., Xiong, Y., Zhang, J.-Y., He, J., Huang, Y., Tao, Z., Xiao, X., 2023. A novel portable smart phone sensing platform based on a supramolecular fluorescence probe for quick visual quantitative detection of picric acid. Anal. Chim. Acta 1254, 341095.

Ilyas, Q., Waseem, M.T., Junaid, H.M., Khan, Z.A., Munir, F., Shaikh, A.J., Shahzad, S.A., 2022. Fluorescein based fluorescent and colorimetric sensors for sensitive detection of TNP explosive in aqueous medium: Application of logic gate. Spectrochim. Acta A 272, 120994.

Kaur, M., Yusuf, M., Tsang, Y.F., Kim, K.-H., Malik, A.K., 2023. Amine/hydrazone functionalized Cd(II)/Zn(II) metal-organic framework for ultrafast sensitive detection of hazardous 2,4,6-trinitrophenol in water. Sci. Total Environ. 857, 159385.

Kayhomayun, Z., Ghani, K., Zargoosh, K., 2022. Synthesis of samarium orthoferrite-based perovskite nanoparticles as a turn-on fluorescent probe for trace level detection of picric acid. Spectrochim. Acta A 281, 121627.

Kostarev, V.A., Kotkovskii, G.E., Chistyakov, A.A., Akmalov, A.E., 2022. Detection of explosives in vapor phase by field asymmetric ion mobility spectrometry with dopant-assisted laser ionization. Talanta 245, 123414.

Kumar, A., Nath, P., Kumar, V., Tailor, N.K., Satapathi, S., 2023. 3D printed optical sensor for highly sensitive detection of picric acid using perovskite nanocrystals and mechanism of photo-electron transfer. Spectrochim. Acta A 286, 121956.

Lambert, S., Bartik, K., Jabin, I., 2020. Specific binding of primary ammonium ions and lysine-containing peptides in protic solvents by hexahomotrioxacalix[3]arenes. J. Org. Chem. 85, 10062–10071.

Lau, Y.H., Rutledge, P.J., Watkinson, M., Todd, M.H., 2011. Chemical sensors that incorporate click-derived triazoles. Chem. Soc. Rev. 40, 2848–2866.

Liu, Y., Sun, Q., Zhou, H., Gao, H., Li, D., Li, Y., 2022a. One-dimensional Europium-coordination polymer as luminescent sensor for highly selective and sensitive detection of 2,4,6-trinitrophenol. Spectrochim. Acta A 264, 120303.

Liu, X., Han, Y., Shu, Y., Wang, J., Qiu, H., 2022b. Fabrication and application of 2,4,6-trinitrophenol sensors based on fluorescent functional materials. J. Hazard. Mater. 425, 127987.

Miranda, A.S., Marcos, P.M., Ascenso, J.R., Berberan-Santos, M.N., Menezes, F., 2022. Anion binding by fluorescent ureido-hexahomotrioxacalix[3]arene receptors: An NMR, absorption and emission spectroscopic study. Molecules 27, 3247.

Mukherjee, D., Das, P., Kundu, S., Mandal, B., 2022, Engineering of graphene quantum dots by varying the properties of graphene oxide for fluorescence detection of picric acid. Chemosphere 300, 134432.

Nguyen, C.H.T., Nguyen, T.H., Nguyen, T.P.L., Tran, H.L., Luu, T.H., Tran, C.D., Nguyen, Q.-T., Nguyen, L.-T.T., Yokozawa, T., Nguyen, H.T., 2023. Aerobic direct arylation polycondensation of N-perylenyl phenoxazine-based fluorescent conjugated polymers for highly sensitive and selective TNT explosives detection. Dyes Pigm. 219, 111613.

Ni, X.L., Tahara, J., Rahman, S., Zeng, X., Hughes, D.L., Redshaw, C., Yamato, T., 2012. Ditopic receptors based on lower- and upper-rim substituted hexahomotrioxacalix[3]arenes: cation-controlled hydrogen bonding of anion. Chem. Asian J. 7, 519–527.

Park, S.Y., Yoon, J.H., Hong, C.S., Souane, R., Kim, J.S., Matthews, S.E., Vicens, J., 2008. A pyrenyl-appended triazole-based calix[4]arene as a fluorescent sensor for Cd^{2+} and Zn^{2+}. J. Org. Chem. 73, 8212–8218.

Qu, B., Mu, Z., Liu, Y., Liu, Y., Yan, R., Sun, J., Zhang, Z., Li, P., Jing, L., 2020. The synthesis of porous ultrathin graphitic carbon nitride for the ultrasensitive fluorescence detection of 2,4,6-trinitrophenol in environmental water. Environ. Sci.-Nano 7, 262–271.

Santra, D.C., Bera, M.K., Sukul, P.K., Malik, S., 2016. Charge-transfer-induced fluorescence quenching of anthracene derivatives and selective detection of picric acid. Chem. Eur. J. 22, 2012–2019.

Sun, X., Wang, Y., Lei, Y., 2015. Fluorescence based explosive detection: from mechanisms to sensory materials. Chem. Soc. Rev. 44, 8019–8061.

Tanwar, A.S., Adil, L.R., Afroz, M.A., Iyer, P.K., 2018. Inner filter effect and resonance energy transfer based attogram level detection of nitroexplosive picric acid using dual emitting cationic conjugated polyfluorene. ACS Sens. 3, 1451−1461.

Teixeira, F.A., Ascenso, J.R., Cragg, P.J., Hickey, N., Geremia, S., Marcos, P.M., 2020. Recognition of anions, monoamine neurotransmitter and trace amine hydrochlorides by ureido-hexahomotrioxacalix[3]arene ditopic receptors. Eur. J. Org. Chem. 13, 1930–1940.

Thippeswamy, M.S., Naik, L., Maridevarmath, C.V., Savanur, H.M., Malimath, G.H., 2022. Studies on the characterisation of thiophene substituted 1,3,4-oxadiazole derivative for the highly selective and sensitive detection of picric acid. J. Mol. Struct. 1264, 133274.

Wang, J., Yang, Y., Sun, G., Zheng, M., Xie, Z., 2019. A convenient and universal platform for sensing environmental nitro-aromatic explosives based on amphiphilic carbon dots. Environ. Res. 177, 108621.

Wang, B.-W., Jiang, K., Li, J.-X., Luo, S.-H., Wang, Z.-Y., Jiang, H.-F., 2020a. 1,1-Diphenylvinylsulfide as a functional AIEgen derived from the aggregation-caused-quenching molecule 1,1-diphenylethene through simple thioetherification. Angew. Chem. Int. Ed. 59, 2338–2343.

Wang, X., Liu, Y., Zhou, Q., Sheng, X., Sun, Y., Zhou, B., Zhao, J., Guo, J., 2020b. A reliable and facile fluorescent sensor from carbon dots for sensing 2,4,6-trinitrophenol based on inner filter effect. Sci. Total Environ. 720, 137680.

Wang, T., Zheng, Q., Zhu, A., Wang, Y., Guo, X., Liu, X., Ying, Y., Wu, Y., Wen, Y., Yang, H., 2022. Construction of Jaffe reaction-based SERS chip for determination of trace picric acid. Sens. Actuators B 368, 132201.

Weiss, J.M., McKay, A.J., DeRito, C., Watanabe, C., Thorn, K.A., Madsen, E.L., 2004. Development and application of pyrolysis gas chromatography/mass spectrometry for the analysis of bound trinitrotoluene residues in soil. Environ. Sci. Technol. 38, 2167–2174.

Wu, C., Wang, C.-Z., Zhu, Q., Zeng, X., Redshaw, C., Yamato, T., 2018. Click synthesis of a quinoline-functionalized hexahomotrioxacalix[3]arene: A turn-on fluorescence chemosensor for Fe^{3+}. Sens. Actuators B 254, 52–58.

Wu, C., Rahman, S., Jiang, X.-K., Wang, C.-Z., Alodhayb, A., Alibrahim, K.A., Georghiou, P.E., Yamato, T., 2023. A fluorescent receptor for alkylammonium ions based on an anthryl-linked triazole-modified hexahomotrioxacalix[3]arene. J. Mol. Struct. 1286, 135615.

Xie, H.-F., Wu, C., Zou, J., Yang, Y.-X., Xu, H., Zhang, Q.-L., Redshaw, C., Yamato, T., 2020. A pyrenyl-appended C_{3v}-symmetric hexahomotrioxacalix[3]arene for selective fluorescence sensing of iodide. Dyes Pigm. 178, 108340.

Zan, Y., Kang, Y., Wang, B., Cui, S., Shen, Z., Shu, J., Kong, X., Chen, L., Yan, X., Li, Y., 2022. Amphiphilic fluorescent nanospheres for quantitative sensing of trinitrophenol in water system. Dyes Pigm. 202, 110296.

Zheng, C., Ling, Y., Chen, J., Yuan, X., Li, S., Zhang, Z., 2023. Design of a versatile and selective electrochemical sensor based on dummy molecularly imprinted PEDOT/laser-induced graphene for nitroaromatic explosives detection. Environ. Res. 236, 116769.

Zhu, P., Lin, L., Chen, W., Liu, L., 2022. Ionic modification on COF with rare earth ions for the selective optical sensing and removal of picronitric acid. Chemosphere 302, 134785.

Figure captions

Scheme 1. The synthetic route of sensor **L**.

Fig. 1. Emission spectra of sensor **L** (1.0 μM) with increasing concentrations of TNP.

Fig. 2. Fluorescence quenching efficiencies ($\eta = (I_0–I)/I_0 \times 100\%$) of **L** (1.0 μM) towards various NACs and potential aromatic interferents.

Fig. 3. Change in absorption spectra of sensor **L** (5.0 μM) with the addition of TNP.

Fig. 4. Frontier-molecular orbital distributions and energy level diagrams for sensor **L** and TNP (calculated at the B3LYP/6-31G(d) level), and the proposed charge transfer mechanism leading to fluorescence quenching.

Fig. 5. Relative energy levels HOMO and LUMO of sensor **L** and various NACs.

Fig. 6. (a) Overlap between excitation/emission spectra of **L** and absorption spectrum of TNP. (b) Overlap between excitation/emission spectra of **L** and absorption spectra of various NACs.

Fig. 7. Partial ^{1}H NMR spectroscopic titration of **L** (3.0 mM) in the presence of increasing amounts of TNP in $CDCl_3$.

Fig. 8. Space-filling of the gas-phase DFT-optimized structures of *left:* sensor **L** showing the π-stacking of the pyrene groups and *right:* 1:1 complex of **L** plus TNP. *Note:* The backbone hydrogen atoms have been removed to ease visualization. Colours: carbon = grey; nitrogen = blue; oxygen= red.

Fig. 9. Photographs (under 365 nm UV light) of the fluorescence response of **L** on test strips after contact with various concentrations of TNP solutions.

Fig. 10. Responses of test strips before (A) and after (B and C) dipping into real water samples, and the responses for contact with TNP crystals (D) and vapour (E).

Table captions

Table 1. Spiked recoveries and RSD (%; n = 3) for detection of different concentration TNP in water and soil samples by sensor **L** and conventional HPLC.

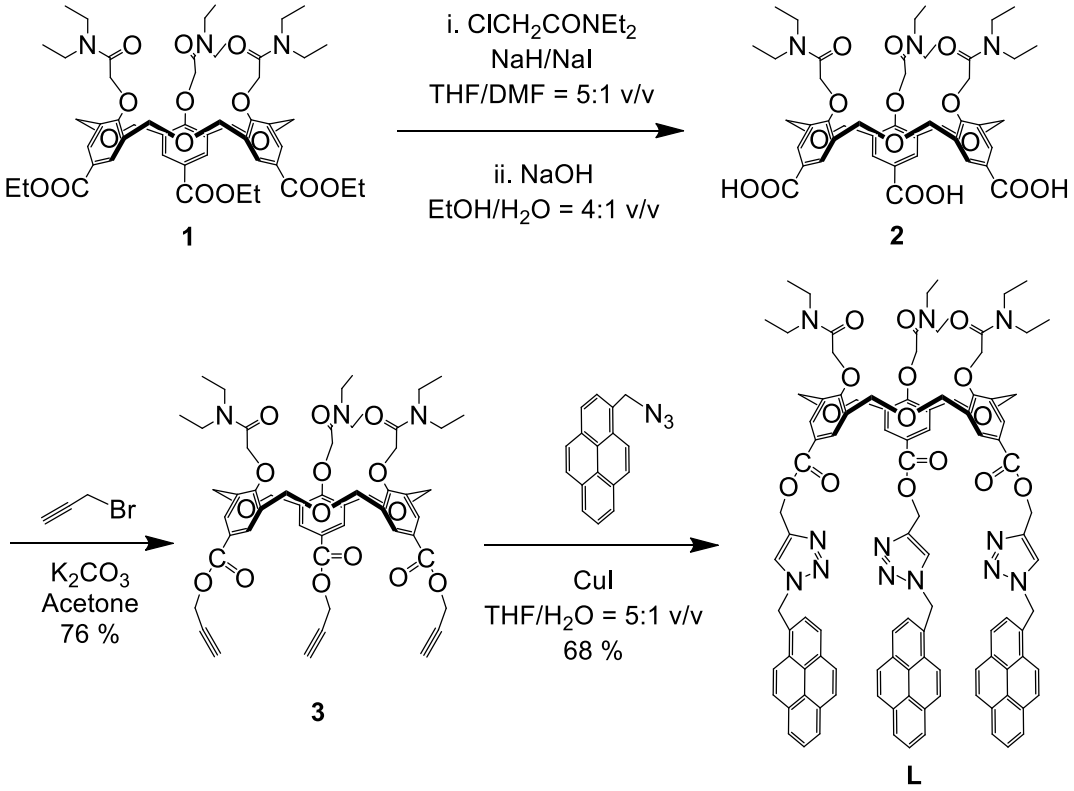

Scheme 1. The synthetic route of sensor **L**.

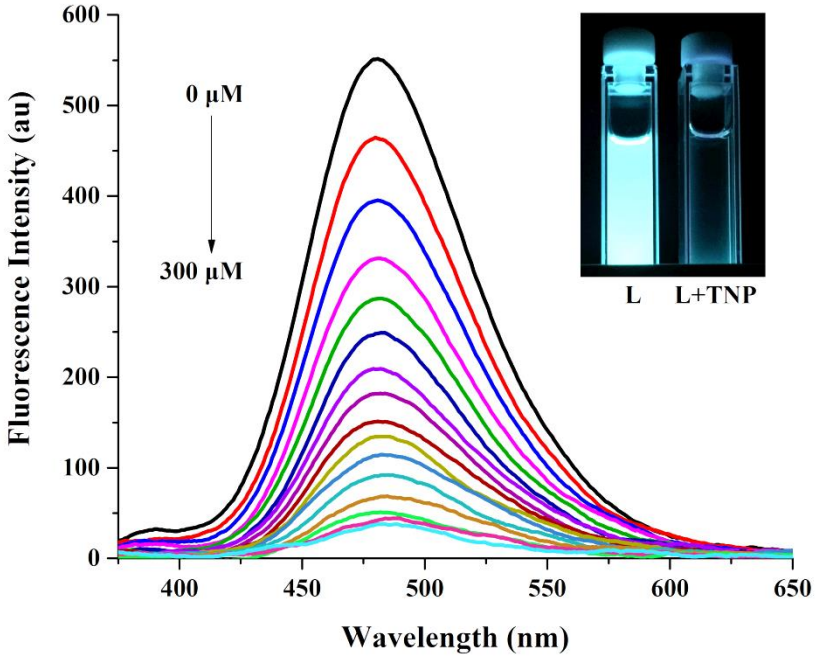

Fig. 1. Emission spectra of sensor **L** (1.0 µM) with increasing concentrations of TNP.

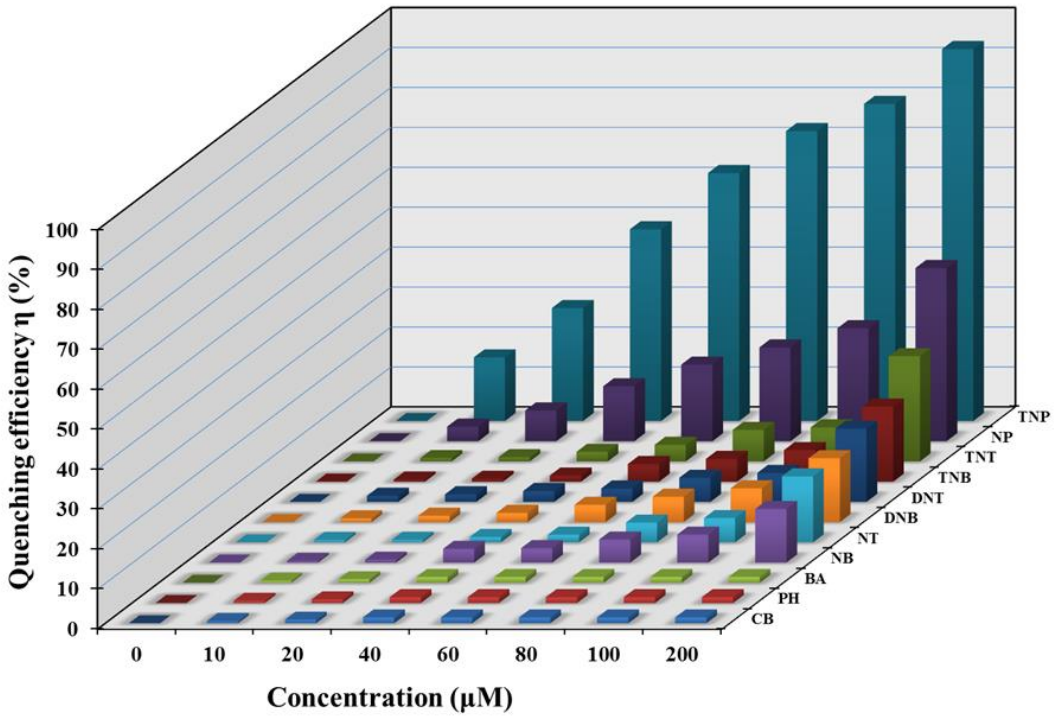

Fig. 2. Fluorescence quenching efficiencies ($\eta = (I_0–I)/I_0 \times 100\%$) of **L** (1.0 μM) towards various NACs and potential aromatic interferents.

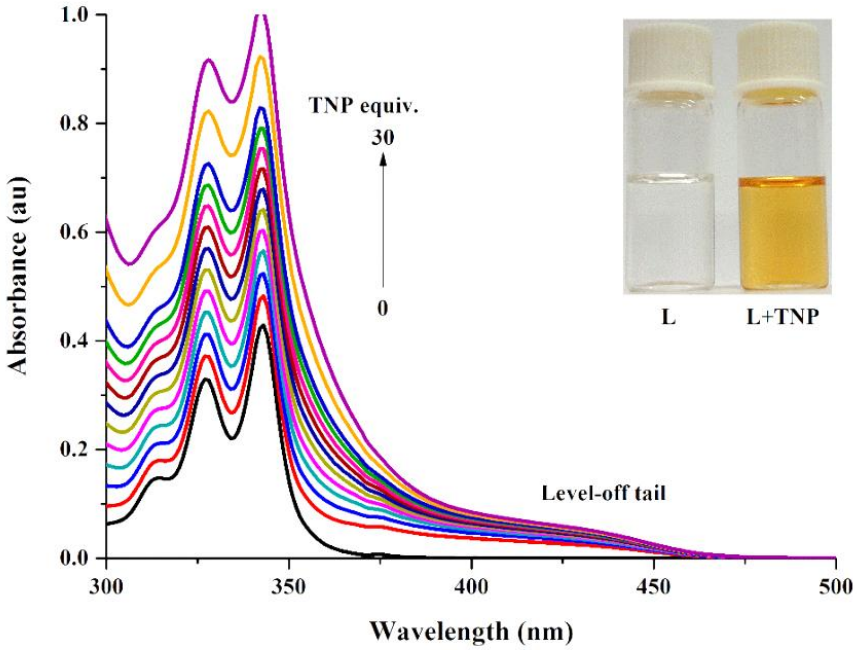

Fig. 3. Change in absorption spectra of sensor **L** (5.0 μM) with the addition of TNP.

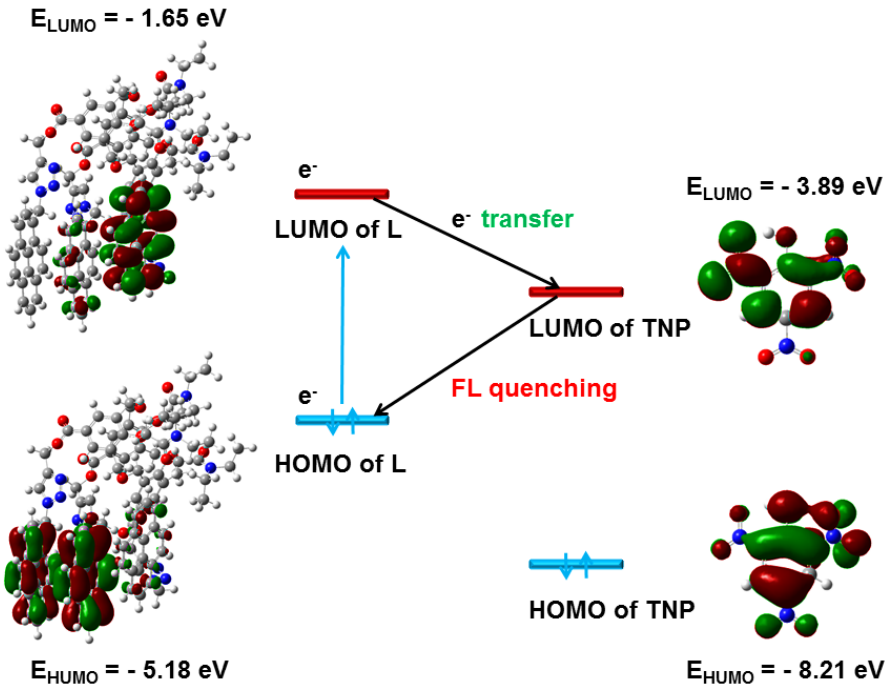

Fig. 4. Frontier-molecular orbital distributions and energy level diagrams for sensor **L** and TNP (calculated at the B3LYP/6-31G(d) level), and the proposed charge transfer mechanism leading to fluorescence quenching.

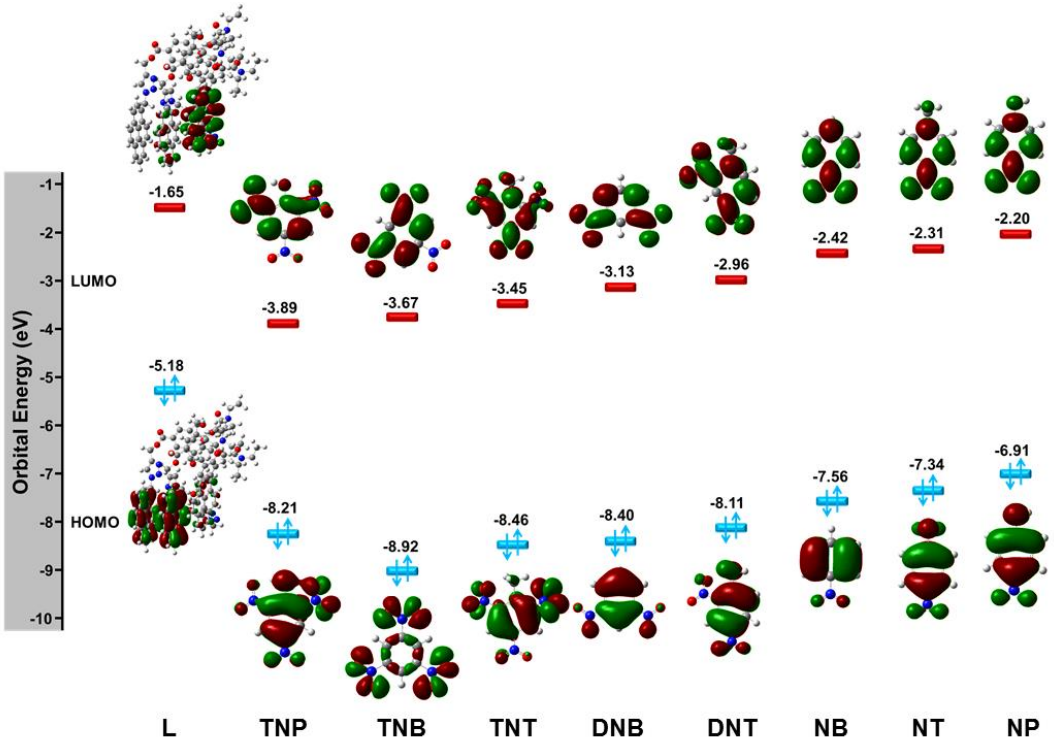

Fig. 5. Relative energy levels HOMO and LUMO of sensor **L** and various NACs.

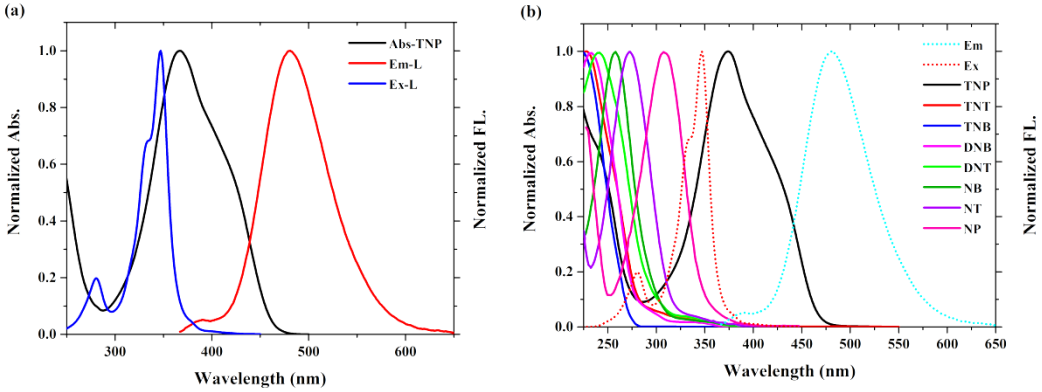

Fig. 6. (a) Overlap between excitation/emission spectra of **L** and absorption spectrum of TNP. (b) Overlap between excitation/emission spectra of **L** and absorption spectra of various NACs.

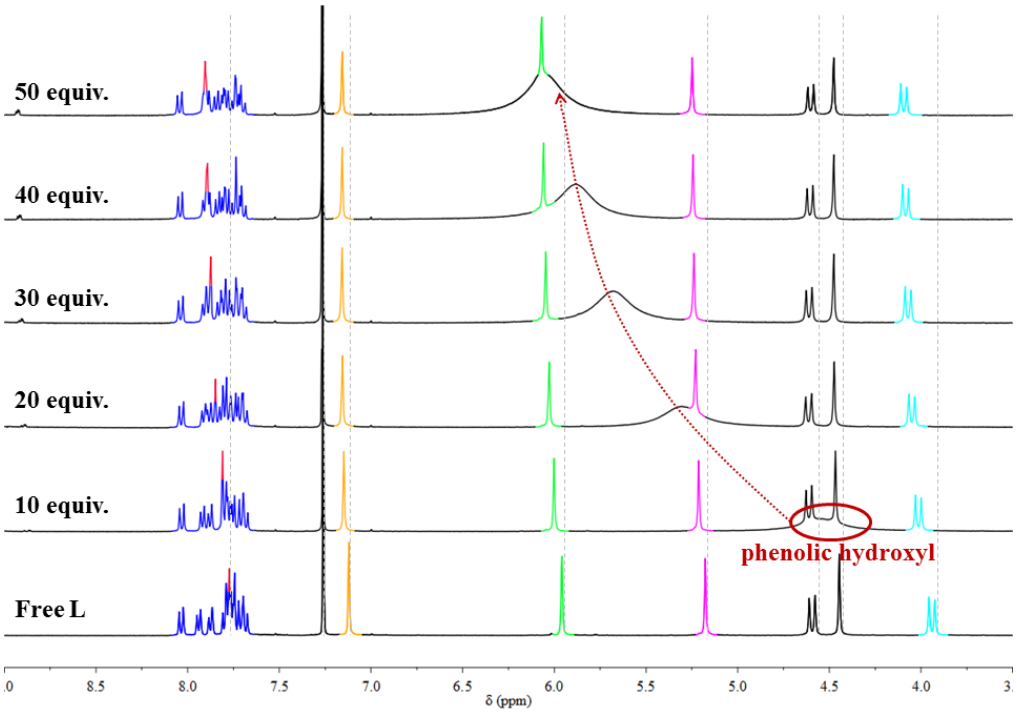

Fig. 7. Partial ^{1}H NMR spectroscopic titration of **L** (3.0 mM) in the presence of increasing amounts of TNP in $CDCl_3$.

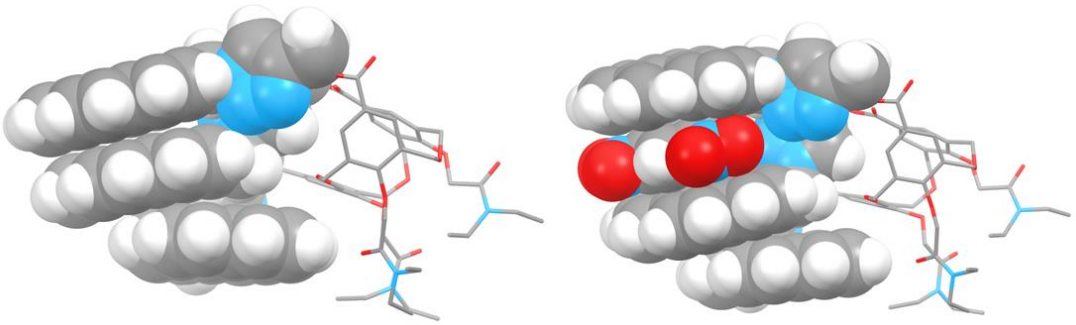

Fig. 8. Space-filling of the gas-phase DFT-optimized structures of *left:* sensor **L** showing the π-stacking of the pyrene groups and *right:* 1:1 complex of **L** plus TNP. *Note:* The backbone hydrogen atoms have been removed to ease visualization. Colours: carbon = grey; nitrogen = blue; oxygen= red.

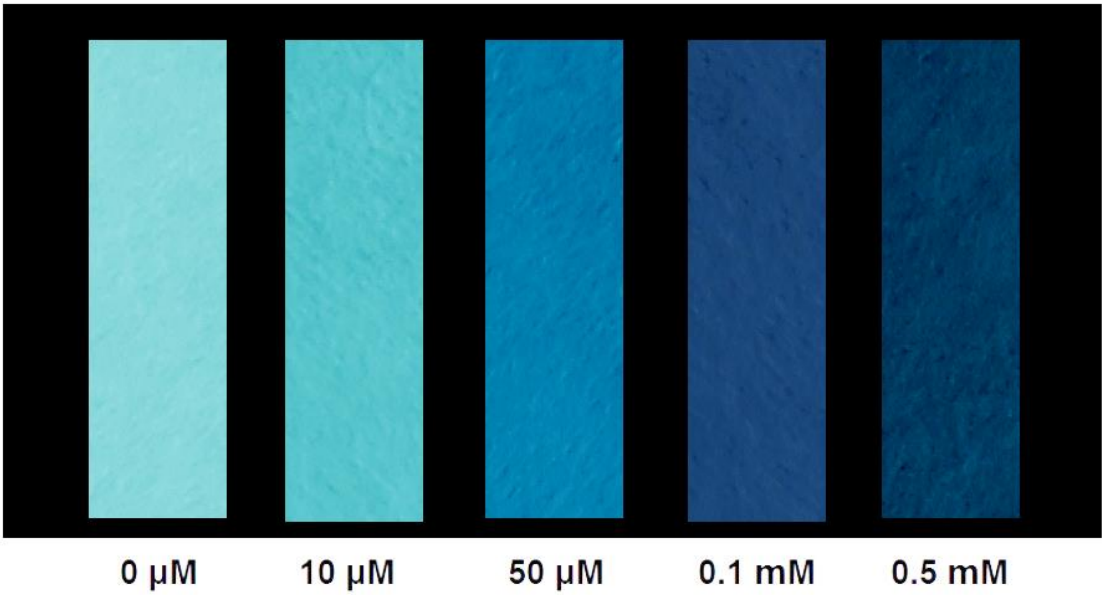

Fig. 9. Photographs (under 365 nm UV light) of the fluorescence response of **L** on test strips after contact with various concentrations of TNP solutions.

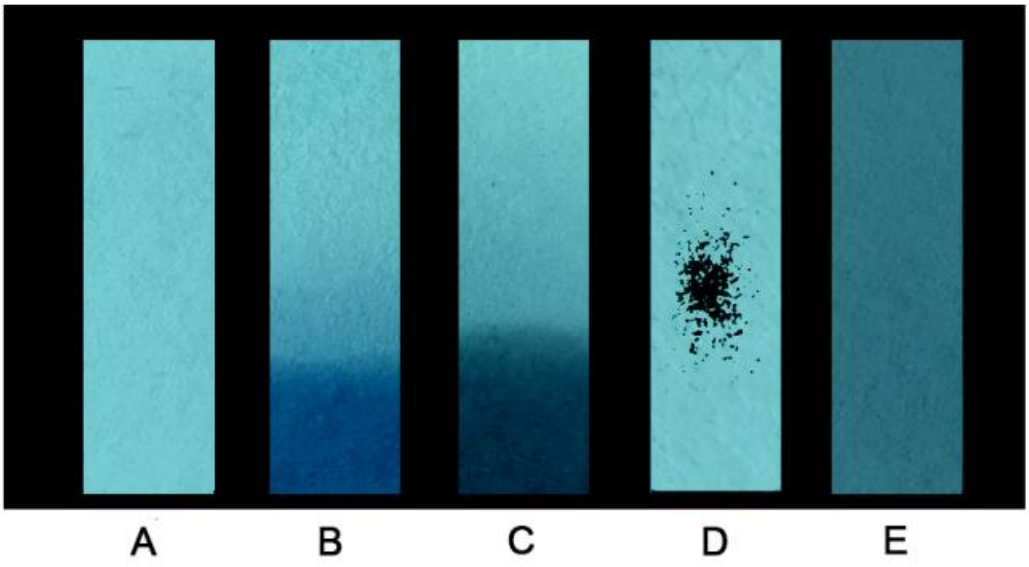

Fig. 10. Responses of test strips before (A) and after (B and C) dipping into real water samples, and the responses for contact with TNP crystals (D) and vapour (E).

Table 1. Spiked recoveries and RSD (%; n = 3) for detection of different concentration TNP in water and soil samples by sensor **L** and conventional HPLC.

Sample	Spiked (μM)	Sensor **L**		HPLC Method	
		Found (μM)	Recovery±RSD (%)	Found (μM)	Recovery±RSD (%)
Tap water	5.00	4.93	98.60 ± 0.89	5.03	100.60 ± 0.54
	10.00	10.08	100.80 ± 0.74	9.94	99.40 ± 0.88
Pond water	5.00	5.16	103.20 ± 1.16	5.12	102.40 ± 1.14
	10.00	10.14	101.40 ± 1.12	9.91	99.10 ± 1.18
Soil	4.36	4.48	102.75 ± 0.83	4.30	98.62 ± 0.43
	8.73	8.48	97.14 ± 1.28	8.86	101.49 ± 0.82

Declaration of interests

☒ The authors declare that they have no known competing financial interests or personal relationships that could have appeared to influence the work reported in this paper.

☐The authors declare the following financial interests/personal relationships which may be considered as potential competing interests:

Author Contributions Statement

Yong-Lang Liu: Investigation, Formal analysis, Writing - review & editing. **Lu-Fang Wu**: Investigation, Formal analysis. **Chong Wu:** Conceptualization, Methodology, Writing - review & editing, Funding acquisition. **Shofiur Rahman**: Computational studies, Writing - review & editing. **Abdullah Alodhayb**: Computational studies. **Carl Redshaw**: Writing - review & editing. **Paris E. Georghiou**: Writing - review & editing. **Takehiko Yamato**: Conceptualization, Writing - review & editing.